UNCLASSIFIED

AD 429239

DEFENSE DOCUMENTATION CENTER

FOR

SCIENTIFIC AND TECHNICAL INFORMATION

CAMERON STATION, ALEXANDRIA, VIRGINIA

UNCLASSIFIED

NOTICE: When government or other drawings, specifications or other data are used for any purpose other than in connection with a definitely related government procurement operation, the U. S. Government thereby incurs no responsibility, nor any obligation whatsoever; and the fact that the Government may have formulated, furnished, or in any way supplied the said drawings, specifications, or other data is not to be regarded by implication or otherwise as in any manner licensing the holder or any other person or corporation, or conveying any rights or permission to manufacture, use or sell any patented invention that may in any way be related thereto.

DASA 1463

Final Report (for Phase V)

INSTRUMENTS FOR MEASUREMENT OF DUSTY AIRBLAST EFFECTS IN HIGH OVERPRESSURE REGIONS

Prepared for:

DEFENSE ATOMIC SUPPORT AGENCY
WASHINGTON 25, D.C.

UNDER CONTRACT DA-49-146-XZ-024
DASA SUBTASK 01.005

STANFORD RESEARCH INSTITUTE

MENLO PARK, CALIFORNIA

*SRI

This report is authorized for open publication by the Department of Defense.

STANFORD RESEARCH INSTITUTE
MENLO PARK, CALIFORNIA

SRI

DASA 1433

September 1963

Final Report (for Phase V)

INSTRUMENTS FOR MEASUREMENT OF DUSTY AIRBLAST EFFECTS IN HIGH OVERPRESSURE REGIONS

Prepared for:

DEFENSE ATOMIC SUPPORT AGENCY
WASHINGTON 25, D.C.

UNDER CONTRACT DA-49-146-XZ-024
DASA SUBTASK 01.005

By: T. D. Witherly

SRI Project No. PIIU-3108

Approved:

R. B. VAILE, JR., DIRECTOR
PHYSICS DIVISION

Requests for copies of this report should be submitted to DDC.
Cameron Station, Alexandria, Virginia, 22314

This research supported by the Defense Atomic Support Agency

Copy No. 3

ABSTRACT

Instrumentation has been developed for the measurement of dynamic pressures and drag forces in high velocity, high pressure airstreams which are laden with dust. The instruments are intended specifically for the high overpressure regions (up to 500 psi) during atmospheric tests of nuclear weapons over desert surfaces.

The development program included the design and construction of:

(1) four total pressure probes (SRI-MAD gages) capable of measuring almost independently the total pressure of the gas phase and the momentum flux of the suspended dust,

(2) four total drag probes to measure directly the drag force on a cylinder,

(3) four dust sampling devices to obtain representative samples of suspended dust for particle size distribution analyses, and

(4) a surface shear gage to measure the magnitude of airblast induced shear stresses in the soil.

Items (1), (2), and (3) were designed for the 50,100,200 and 500 psi overpressure regions, one of each item for each pressure. Item (4) was designed for the 200 psi overpressure region.

Additional tests will be required on items (1) and (4) before they can be used in the field.

CONTENTS

ILLUSTRATIONS

TABLES

I INTRODUCTION

During nuclear weapons tests over desert regions such as the Nevada Test Site (NTS) it has been observed that large quantities of dust are raised from the surface and carried in suspension with the airblast. When this occurs the pattern of the air flow may be significantly altered by the presence of the dust, errors may be introduced into the measurement of dynamic pressures by conventional methods, and the dust itself may contribute significantly to target damage.

To better understand the flow phenomena associated with dusty airblasts and the forces experienced by exposed drag sensitive targets, Stanford Research Institute (SRI), under the sponsorship of the Defense Atomic Support Agency (DASA) has performed a comprehensive series of theoretical and laboratory studies dealing with particle laden gas flows under Contract DA-49-146-XZ-024.

The entire program was conducted in five phases. In Phase I several total pressure probes that had been used in field tests were calibrated in SRI's "dusty" wind tunnel to determine their sensitivity to dust. Phase II was a theoretical study of the effects of suspended particulate matter in steady incompressible, subsonic flow around cylinders and spheres. The theories developed in Phase II were tested experimentally in Phase III for validity and range of applicability. In Phase IV the theory was extended to cover rectangular bodies and to include the effects of compressibility and unsteadiness of flow.

This report covers Phase V of the program, in which the instruments for field test measurements of dusty airblast effects in high overpressure regions have been designed and prototypes constructed. The following three types of measuring instruments were developed:

(1) a total pressure probe designed to measure almost independently the dynamic pressure of the air phase and the momentum flux of the suspended particulate matter;

(2) a total drag probe for measuring directly the total drag force on a cylindrical body; and

(3) a subsurface shear gage for measuring airblast induced ground surface shear forces.

Four each of the total pressure probes, designated SRI-MAD gages (for measurement of air and dust), and total drag probes were designed and constructed for use in the 50, 100, 200, and 500 psi overpressure regions, respectively. The interpretation of data from the MAD gages requires a knowledge of dust particle size distribution. Therefore, a device was developed also for obtaining representative samples of the suspended dust. Four of these dust samplers were constructed to be used in conjunction with the MAD gages. One surface shear gage, designed for the 200 psi overpressure region, was constructed.

The MAD gages were patterned after a design previously developed at SRI for use in subsonic flow. The original gage had been calibrated in the SRI subsonic "dusty" wind tunnel and experimental results were in agreement with predicted behavior.[1]* Analytical and experimental data from this earlier program can be used to predict the response of one of the current gages, designed for the 50 psi region where the flow is subsonic (see Table 1). Since the other current MAD gages were designed for overpressure regions in which supersonic flow obtains, the subsonic tunnel was inadequate for calibration purposes.

For these gages an electrical analog (with particle size and free stream velocity as variables) was developed to predict the response to dust, and a series of rocket sled tests at high supersonic velocities (up to Mach 2) were conducted to test the dynamic behavior in clean and dusty air. Artificially created dust clouds of known density were used in the sled tests to simulate dusty airblast phenomena.

The total drag probes and the surface shear gage were calibrated statically in the laboratory.

---

* Numbered references are listed at the end of this report.

II SUMMARY, CONCLUSIONS, AND RECOMMENDATIONS

The instrumentation developed on this project is suitable for use in high velocity, high pressure air streams which are laden with dust. The research was undertaken to provide means of measuring dynamic pressure and dust momentum flux in regions where the flow is supersonic, and to provide experimental means of measuring surface shear and of checking theoretical estimates of the total drag on a cylindrical body.

The development program included:

(1) The design and fabrication of four total pressure probes (SRI-MAD gages) designed to measure almost independently the air phase dynamic pressure and the dust momentum flux.

(2) The design and fabrication of four devices for capturing samples of the suspended dust for particle size analysis (needed in the interpretation of MAD gage data).

(3) The design and fabrication of four total drag probes to measure the drag force on a cylindrical body.

(4) The design and fabrication of a gage for measuring airblast induced surface shear forces.

Items (1), (2), and (3) were designed for each of four overpressure regions, 50, 100, 200, and 500 psi; item (4) was designed for the 200 psi overpressure region.

The total drag probes and shear gage were calibrated in the laboratory. In the absence of a suitable laboratory facility for calibrating the MAD gages, an analog computer program was developed to predict their response to dust as a function of dust particle size and free stream velocity. A series of rocket sled tests was undertaken to test the dynamic behavior of the MAD gages in clean and dusty air.

The calibration of the drag probes and shear gages indicates that these instruments cover adequately the range of loadings for which they were intended. As test conditions are now envisioned, the sensitivities and response times of the instruments are also entirely adequate. The

calibrations were performed to check design and fabrication procedures rather than to provide working calibration curves. Final calibrations should be conducted with the instruments connected to their associated electronics.

The time response of the MAD gage, particularly with respect to dust, is difficult to determine in the laboratory since it is a dynamic instrument. Indications are that the rise time in response to a step input is about 10 or 12 milliseconds for air dynamic pressure, and about 4 or 5 milliseconds for dust momentum flux. It is probable that some improvement will be necessary for field tests. This can be done by filling some of the pressure passages with low-compressibility fluid such as silicone oil or grease during assembly.

The design concept of the MAD gage is the same as that for the subsonic gage developed previously (Ref. 1) and their geometries are quite similar. There is no reason to believe that the analytical and experimental work done at that time cannot be used to predict the behavior of the MAD gage that is designed for use in the 50 psi overpressure region where the flow is supersonic.

The dust response data from the rocket sled tests were inconclusive and failed to either prove or disprove the validity of the analog solutions for dust registry coefficients in supersonic flow.

The sled tests produced only negative results with respect to clean air behavior and disclosed the necessity for a design modification.

A unique feature of the MAD gage design is the incorporation of a static pressure port to enable the front transducer to sense the difference between total and static pressures. In this way the dynamic pressure can be measured directly in one instrument at one location, rather than by correlating total pressure measurements from one instrument with static pressure measurements from another instrument nearby. It is evident from the track test clean air data that the static port is not sensing true static pressure. Some additional experimentation will be necessary before this desirable feature of measuring dynamic pressure directly can be incorporated in the gage.

There are at least three practical approaches to the problem. The simplest but least attractive, perhaps, would be to revert to the original design in which the front transducer measured total pressure only and static pressure was measured by another instrument independently. This could be accomplished by simply plugging the static ports. A second approach would be to calibrate the gages for static pressure error as a function of velocity and angle of attack. It may be possible, by minor relocation of static pressure ports, to make the gages insensitive to angle of attack. A third approach would be to relocate the static ports to locations where they sensed true static pressure. This would necessitate lengthening the probes (a relatively simple task) or creating a static pressure area in the near vicinity of the MAD gage, perhaps in conjunction with the mounting bracket. The second and third approaches would each require a limited amount of experimentation in a supersonic wind tunnel or on a rocket sled track.

It is recommended that this apparent deficiency in the MAD gage be investigated by a combination of approaches two and three. If a promising method of obtaining dust response data can be devised (perhaps by a sled-borne tape recorder) the investigations of dust registry coefficients and clean air behavior should be combined in one experimental program. If the investigation is to be restricted to clean air behavior experimentation in a supersonic wind tunnel would be more efficient.

In the latter case, that is, in the absence of an experimental program to determine dust response, it will be necessary to rely on the analog solution for the determination of dust registry coefficients.

It should be realized that the instruments developed in this program differ substantially from instrumentation used heretofore. The shear gage, in addition, will be used in a new area of investigation where phenomena are not clearly defined. When the instruments are used in the field for the first time it would be highly desirable to deploy as many of each type as possible to provide cross-checks. In the case of the shear gage it would be desirable also to conduct preliminary laboratory type tests to help establish orders of magnitude and to investigate methods of gage deployment.

III EXPERIMENTAL WORK

A. Design Operating Conditions

The prediction of field test operating conditions (i.e., flow Mach number and dust loading) for the various overpressure regions was based on data contained in Refs. 2, 3, and 4. The predicted values of flow Mach number, clean air dynamic pressure (q_{air}), and maximum dust momentum flux (ϕ_{dust}) are given in Table I.

Table I

PREDICTED FIELD TEST OPERATING CONDITIONS

Overpressure (psi)	Flow Mach Number	q_{air} (psi)	ϕ_{dust} (psi)
50	0.95	32	96
100	1.25	112	336
200	1.50	308	924
500	1.88	1075	3225

In estimating the errors in drag and shear force measurements due to motion of the ground mass it was assumed that the horizontal acceleration of the ground mass would not exceed 10 g in the area of interest.

B. Design of the MAD Gage

1. Description

The SRI-MAD gage (see Fig. 1) is a modification of a gage developed previously at SRI for use in subsonic flow regimes. It consists of a vented pitot tube about 6-inches-long with ports for measuring the local pressure at two locations along the tube's length. Pressure is measured as near the forward end of the tube as possible, and again as near the rear as possible. Free stream static pressure is measured through static taps in the wall of the gage at an appropriate distance aft of the nose.

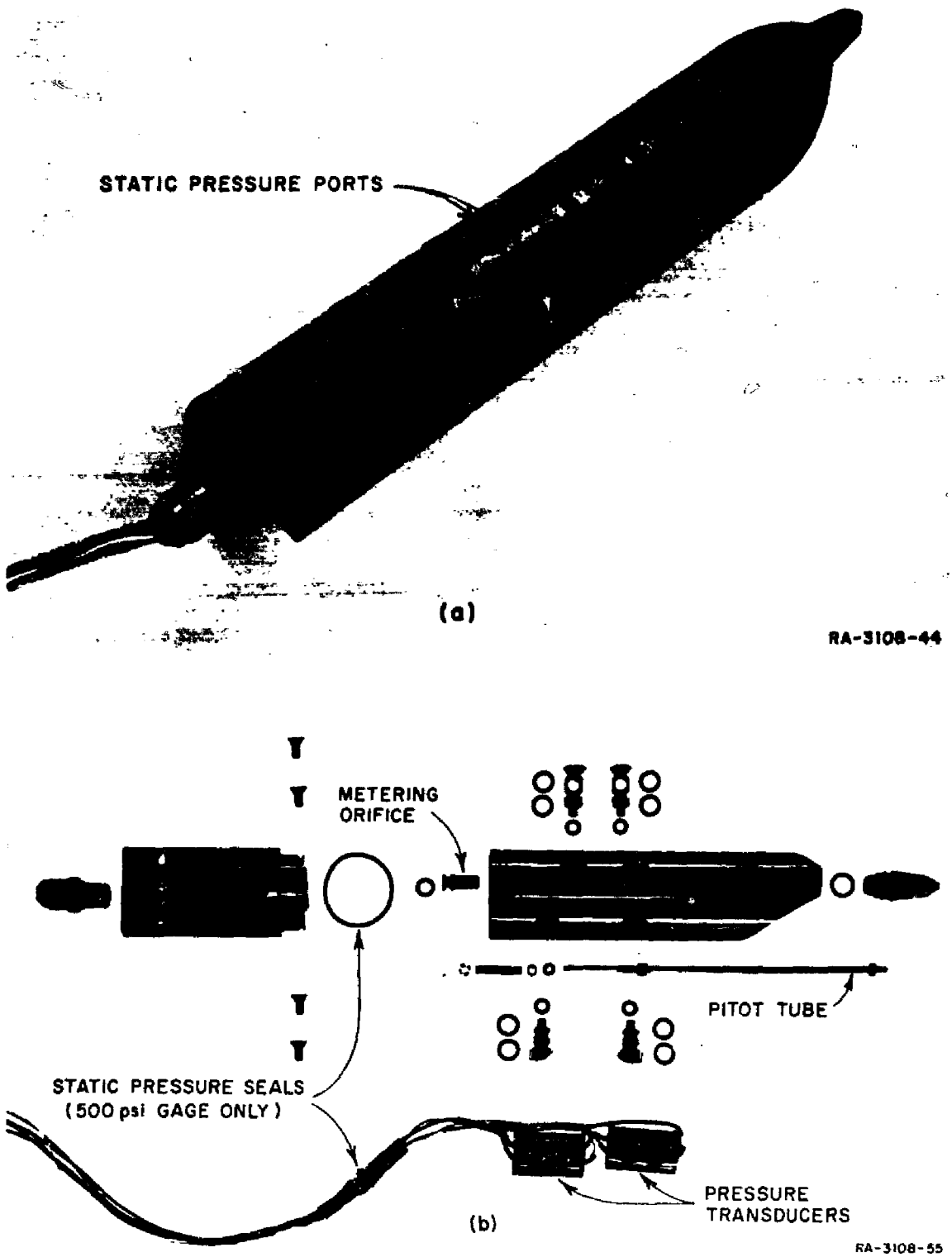

FIG. 1 SRI-MAD GAGE: (a) ASSEMBLED GAGE, (b) GAGE COMPONENTS

The pressures from the front and rear ports are transmitted through separate passages to two Ultradyne variable reluctance pressure transducers arranged in such a way that the front transducer senses the difference between the front port pressure and static pressure, while the rear transducer senses the difference between the front and rear port pressures. Venting of the pitot tube (to avoid plugging with dust) is controlled by a metering orifice at the rear of the tube. The error in total measurement due to venting of the pitot tube is less than 1% for all free stream velocities of interest.

The design details and calculations for the MAD gage are given in Appendix A.

2. Theoretical Performance

As the stream of dust laden air impacts on the nose of the tube, the air phase decelerates almost immediately to the velocity of the metered airflow within the tube. The dust particles being considerably more massive decelerate gradually due to air drag, slowly transfer momentum to the air, and cause a corresponding increase in pressure with distance along the tube's length.

Ideally the dust particles would not decelerate at all before passing the first port, and would have decelerated to air velocity before reaching the rear port. If this were the case the front pressure transducer would register air phase dynamic pressure only, while the rear transducer would reflect the total dust momentum flux. Unfortunately, these phenomena can only be approached in reality. A finite deceleration of lighter particles ahead of the forward tap cannot be avoided, and particle velocity inside the tube approaches air velocity asymptotically.

A detailed theoretical analysis of the behavior of an idealized model in subsonic flow is given in Ref. 1 where the capture efficiency, e, and dust registry coefficient, N, are plotted for each of two assumed probe geometries and for various free stream Reynolds numbers.

In supersonic flow, for which three of the present MAD gages have been designed, a shock wave stands ahead of the mouth of the tube. The

shock detachment distance is so short that even the lightest of particles cannot have their trajectories changed appreciably and virtually all particles directed toward the mouth of the tube in the free stream are captured. Thus, the capture efficiency loses its significance in supersonic flow. However, the analysis of the gage's behavior with respect to the dust registry coefficients at the front and rear ports becomes more complex.

Directly behind the shock wave (where the air phase has become subsonic) the dust particles, still traveling at nearly free stream velocity, are usually supersonic relative to the surrounding air. Furthermore, the air phase is undergoing rapid and drastic property changes. Under these conditions, calculation of particle deceleration rates is extremely difficult.

Preliminary analyses of particular extreme conditions indicated that for some free stream conditions of interest the small particles would decelerate appreciably before reaching the front port of the gage, while for other free stream conditions the large particles would not decelerate sufficiently before reaching the rear port. Since the function of the MAD gage is to measure independently the air phase dynamic pressure and the dust momentum flux, it is necessary to know to what extent the dust contributes to the forward port pressure and to what degree the rear port pressure fails to reflect all of the dust momentum flux. A suitable calibration facility was not available and analytical determinations for particular conditions are tedious and time consuming. Therefore, the problem of predicting the MAD gage's response to dust of different particle sizes and at different free stream velocities was handled on an electrical analog computer. The theoretical analysis and the analog computer program are described in Appendix B.

3. Testing and Calibration

The dynamic testing of the MAD gages was conducted on the Supersonic Test Track at the Air Force Missile Development Center (AFMDC), Holloman Air Force Base, New Mexico. Specific objectives of the test were to check the behavior of the gages as supersonic pitot tubes in clean air, including

their sensitivity to angles of attack and yaw, and to spot-check the analog computer solutions for dust registry coefficients. An incidental objective was to check the tendency of the gages to plug as dust was encountered.

The rocket sled and the deployment of MAD gages is shown in Fig. 2. MAD gage A, designed for the 50 psi overpressure in field tests, was mounted in the center with its axis aligned with the flow streamlines; gage B, designed for 100 psi overpressure, was mounted on the starboard side at a 10^{0} angle of attack; and gage C, designed for 200 psi overpressure, was mounted on the port side at 10^{0} angle of yaw. MAD gage D, designed for the 500 psi overpressure region, was not sufficiently sensitive to be used in track tests.

Dust loading in the track tests was simulated by artificially created dust clouds. The generators used for this purpose are shown in Fig. 3. Dust was introduced at a metered rate into the high velocity throat section of a convergent-divergent duct. The mixture of air and dust, contained in a frangible polyethylene duct, was then directed across the path of the oncoming sled. Metering was accomplished by spreading a measured amount of dust evenly on a porous cloth conveyer belt (see insert, Fig. 3). A few seconds prior to the sled's arrival, a signal was provided to start the belt which then proceeded at a known rate. At the throat section of the air duct, the belt passed over a slotted hollow idler pulley where a secondary airstream was used to blow the dust off the belt and into the air duct. Two dust generators were used in tandem (about 3 feet apart) to increase retention time. Four types of dust were used at each of two sled velocities, 1200 ft/sec and 1600 ft/sec. When the dust generators were placed at the track station where sled velocity was 1200 ft/sec the MAD gages were exposed to dust loading for about 7-1/2 milliseconds; when placed at the 1600 ft/sec station, exposure time was about 5-1/2 milliseconds. A total of 13 tests were conducted with peak velocities approaching Mach 2. Meaningful clean air data were obtained in 10 of the tests, eight of which involved dust loading.

The clean air response of the MAD gages is shown in Fig. 4 where the average pressure readings from the MAD gages are compared with the computed dynamic pressure for the test conditions. Unfortunately, the dust response

FIG. 2 ROCKET SLED SHOWING SRI-MAD GAGE DEPLOYMENT: (a) ROCKET SLED, (b) MOUNTING OF MAD GAGES, (c) SHOCK PATTERN AROUND MAD GAGES

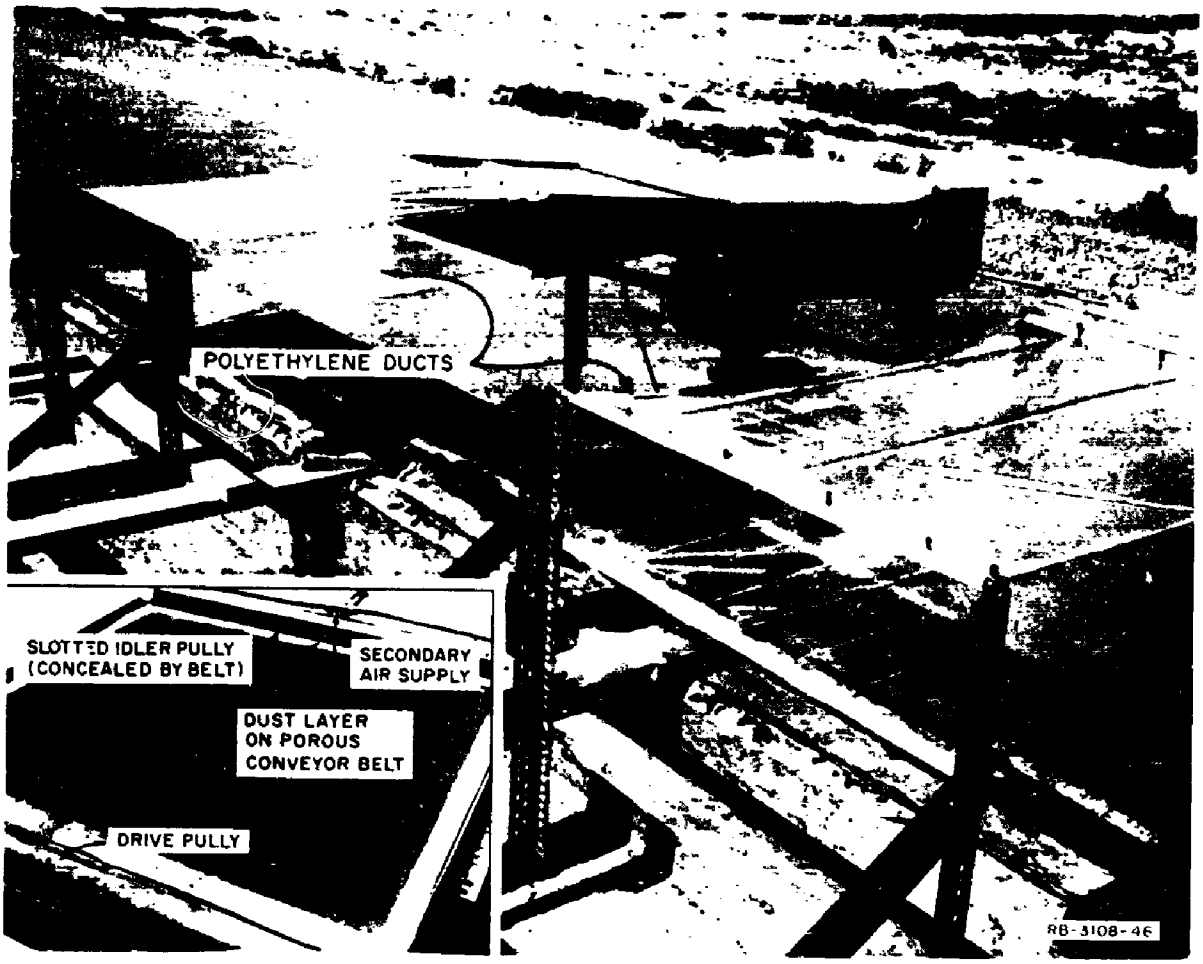

FIG. 3 DUST CLOUD GENERATORS FOR TRACK TESTS

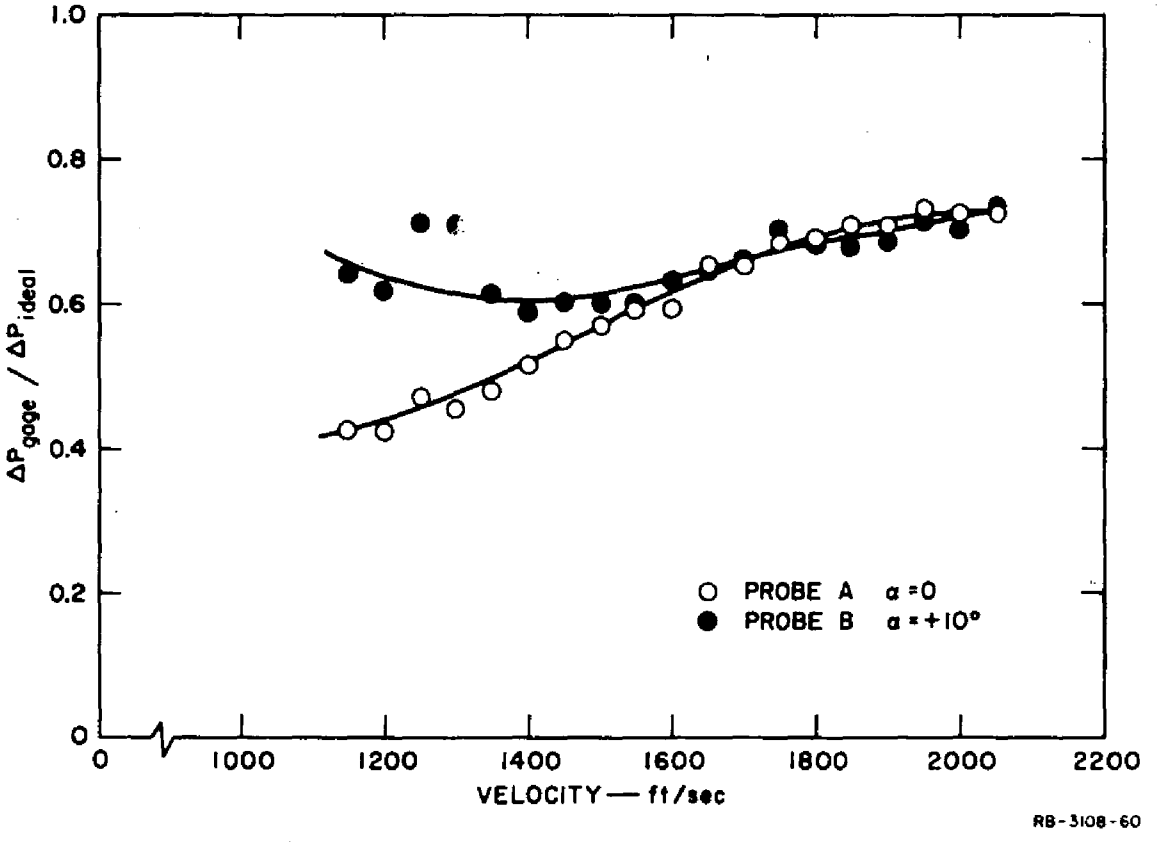

FIG. 4 MAD GAGE CLEAN AIR RESPONSE IN ROCKET SLED TESTS

data were not conclusive due to insufficient dust generation and inadequacy of the telemetry system (see discussion, Appendix C).

Test conditions and calculations of air dynamic pressure and dust momentum flux are given in Appendix C.

C. Design of the Total Drag Probe

1. Description

The drag sensitive target in the total drag probe is a hollow 3-inch-long section of a 3-inch-diameter mounting cylinder 33 inches long over-all. To minimize end effects, the mounting cylinder is machined to the exact diameter of the target cylinder for a distance equal to about two diameters on either side of the target. The target cylinder is restrained axially by set screws to avoid fouling at the ends. When in use the cylinder is mounted with its longitudinal axis horizontal and normal to the direction of air flow.

The basic design of the probe is illustrated in Fig. 5. An octagonal proving ring inside the hollow target cylinder is used to measure the total drag force. This strain sensing element extends the full length of the hollow target element, providing support and alignment.

Two strain gages, one near each end of the sensing element, are used in series in each leg of a four leg bridge to obtain a measurement of the total drag force acting on the target cylinder.

Detailed design calculations for the total drag probes are outlined in Appendix A. Primary consideration was given to minimizing errors due to horizontal acceleration of the ground, and to increasing the natural frequencies of the probes (thereby reducing their rise time). Optimizing on these two parameters, while at the same time designing for adequate structural strength, suggested the use of different materials for different probes. Consequently, probes A and B, designed for the 50 and 100 psi overpressure regions, respectively, are all aluminum; probe C, designed for the 200 psi overpressure region, has a steel target cylinder with an aluminum strain sensing ring; and probe D, designed for the 500 psi overpressure region, is all steel. The mounting cylinders are steel for all probes.

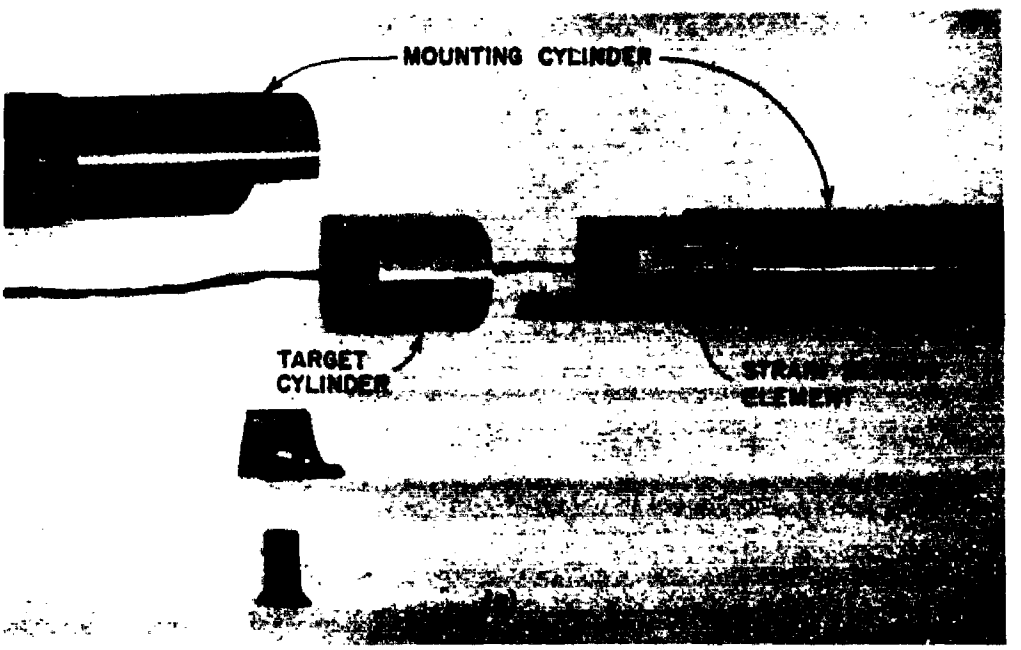

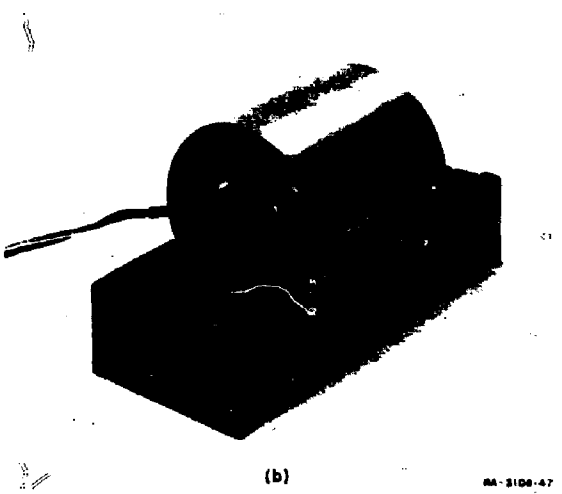

(b)

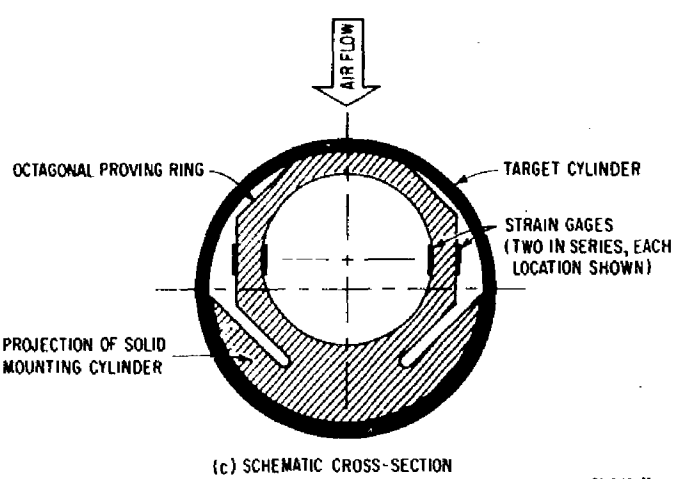

(c) SCHEMATIC CROSS-SECTION

FIG. 5 TOTAL DRAG PROBE ASSEMBLY: (a) EXPLODED VIEW – DRAG PROBE SHOWN IS FOR 50 psi OVERPRESSURE REGION, (b) 500-psi PROBE SHOWN ON CALIBRATING JIG, (c) SCHEMATIC CROSS-SECTION

The error to be expected from accelerations of the ground mass is in all cases less than 0.5% of the anticipated maximum drag force. The natural frequencies of the probes vary from about 4 kc for probes A and B to 5-1/2 kc for probe D.

2. Calibration

The total drag probes were calibrated statically in the laboratory using a Baldwin Tate Emory testing machine to supply the loading force and a Baldwin Lima Hamilton strain indicator to measure the resulting strain. The calibration curves for the four total drag probes are shown in Fig. 6. The sensitivity of each gage provides for measurements as low as 1% of design loads, and dust loadings up to five times the expected air loading can be tolerated without exceeding elastic limits.

D. Design of the Dust Sampler

1. Description

A typical dust sampler is shown in Fig. 7. It consists of a 2.00-inch I.D. cylindrical tube open fore and aft and aligned with the blast streamlines. For field tests the tubes will be equipped with explosive closing devices about 20 inches apart in tandem. On signal (initiated, probably, by the advancing shock wave) the devices will fire simultaneously, pinching off a section of the tube in the form of a sausage and capturing a sample of dust laden air. Small holes are provided to bleed off the overpressure before the tubes are opened to remove the dust sample. The function of the samplers is to obtain representative samples for determining particle size distribution; the measurement of dust loading, i.e., the mass ratio of dust to air, is the function of the MAD gage.

The obvious advantage of the dust sampler design is its simplicity. In supersonic flow, isokinetic sampling can be achieved if the shock wave is made to attach to the forward end of the tube since the particle trajectories are then undisturbed until the tube entrance is reached. It is necessary that velocity equilibrium between dust and air be re-established before reaching the location of the first device and that the two closures are accomplished simultaneously. With these ideas in mind the leading edges of the tubes are sharpened to minimize the shock

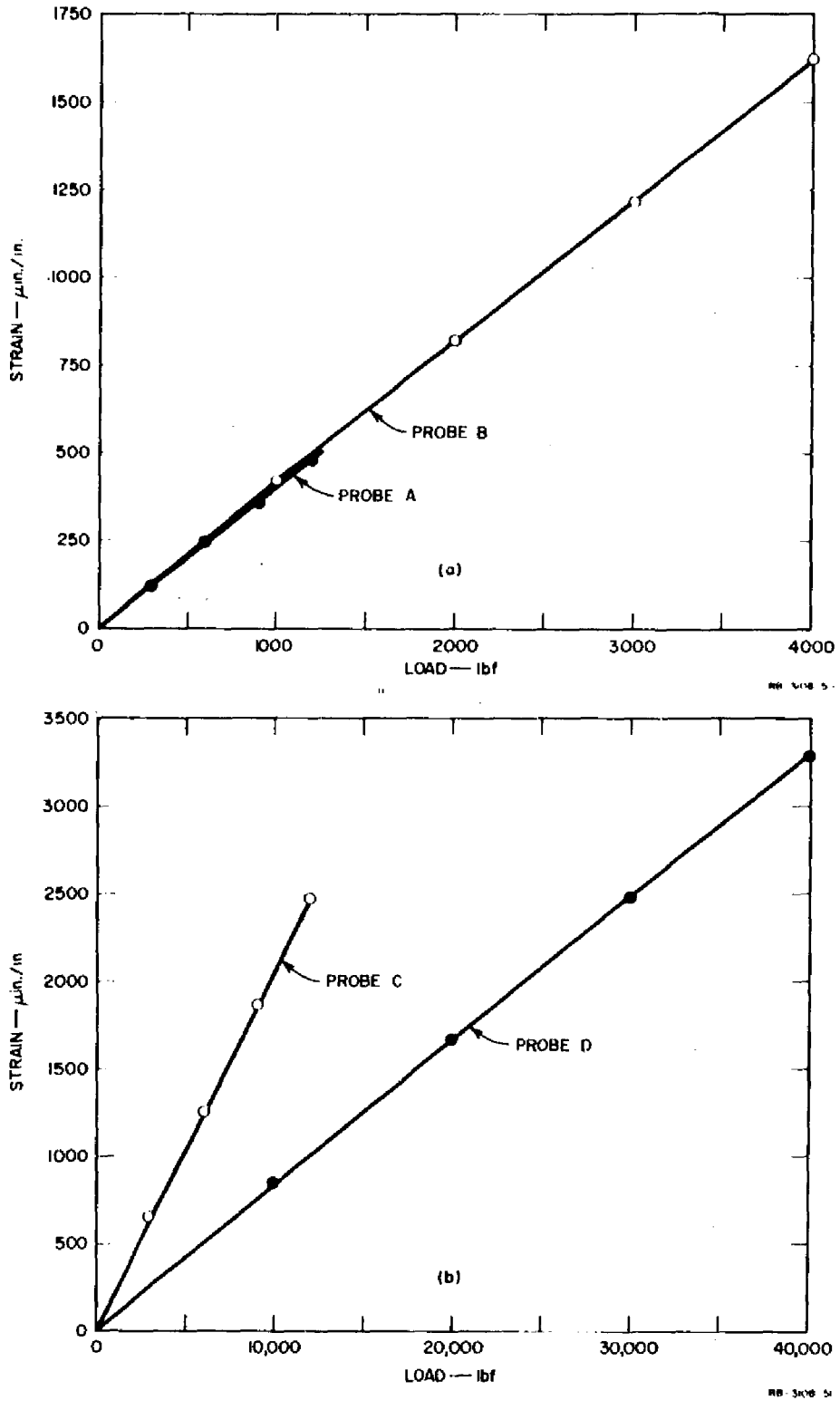

FIG. 6 TOTAL DRAG PROBE CALIBRATIONS-STRAIN vs. LOADING FORCE: (a) PROBES A AND B, (b) PROBES C AND D

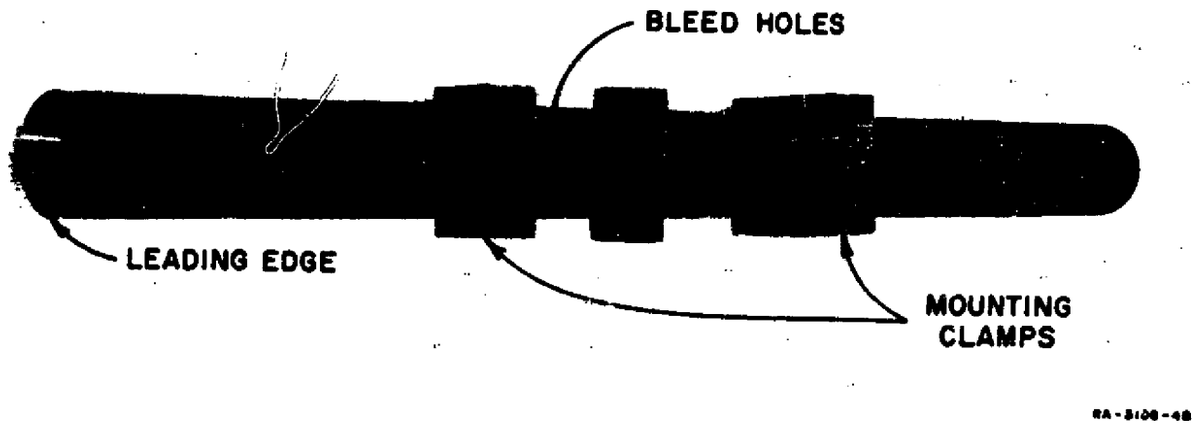

FIG. 7 DUST SAMPLER (Explosive Closures Not Shown)

detachment distance and the first device can be placed about six diameters aft of the leading edge. It is estimated from calculations for the MAD gage that equilibrium is re-established within about three diameters (see Appendix B). The tube walls comply with specifications for an existing closure system that has been tested extensively and used successfully in field tests. The manufacturer of the explosive devices (Lockheed Missiles and Space Company) advises that initiation of the closures can be controlled within ± 1/4 microseconds, and the completion of closure controlled to within ± 1 or 2 microseconds, depending on the selection of high explosive. The time for closure is about 30 microseconds.

The details of the dust sampler design are given in Appendix A.

E. Design of the Surface Shear Gage

1. Description

The basic design of the surface shear gage is shown in Fig. 8. It consists of a flat aluminum plate 1-foot-square supported on two octagonal half-rings similar to the one full ring used in each total drag probe. The strain rings in turn are fastened to a steel mounting plate. The purpose of the gage is to measure airblast induced shear forces at a ground plane near the surface sufficiently deep that the covering soil will remain in place. When in use the assembly will be placed in a horizontal plane under the surface of the ground with the longitudinal axes of the half-rings normal to the direction of blast.

Two strain gage bridge circuits are used in the surface shear gage to obtain independent measurements of normal and shear forces. The placement of the strain gages and their electrical connections are shown schematically in Fig. 9. As in the total drag probes each leg of the Wheatstone bridges contains two strain gages in series, one mounted at each end of the strain sensing element.

The surface shear gage was designed for a shear stress of 40 psi. The natural frequency of the gage itself is about 2600 cps and the error due to ground motion (assuming a maximum acceleration of the ground mass of 10 g) is less than 1%. It should be realized that an indeterminate amount of soil will move with the gage and increase its effective mass to some extent.

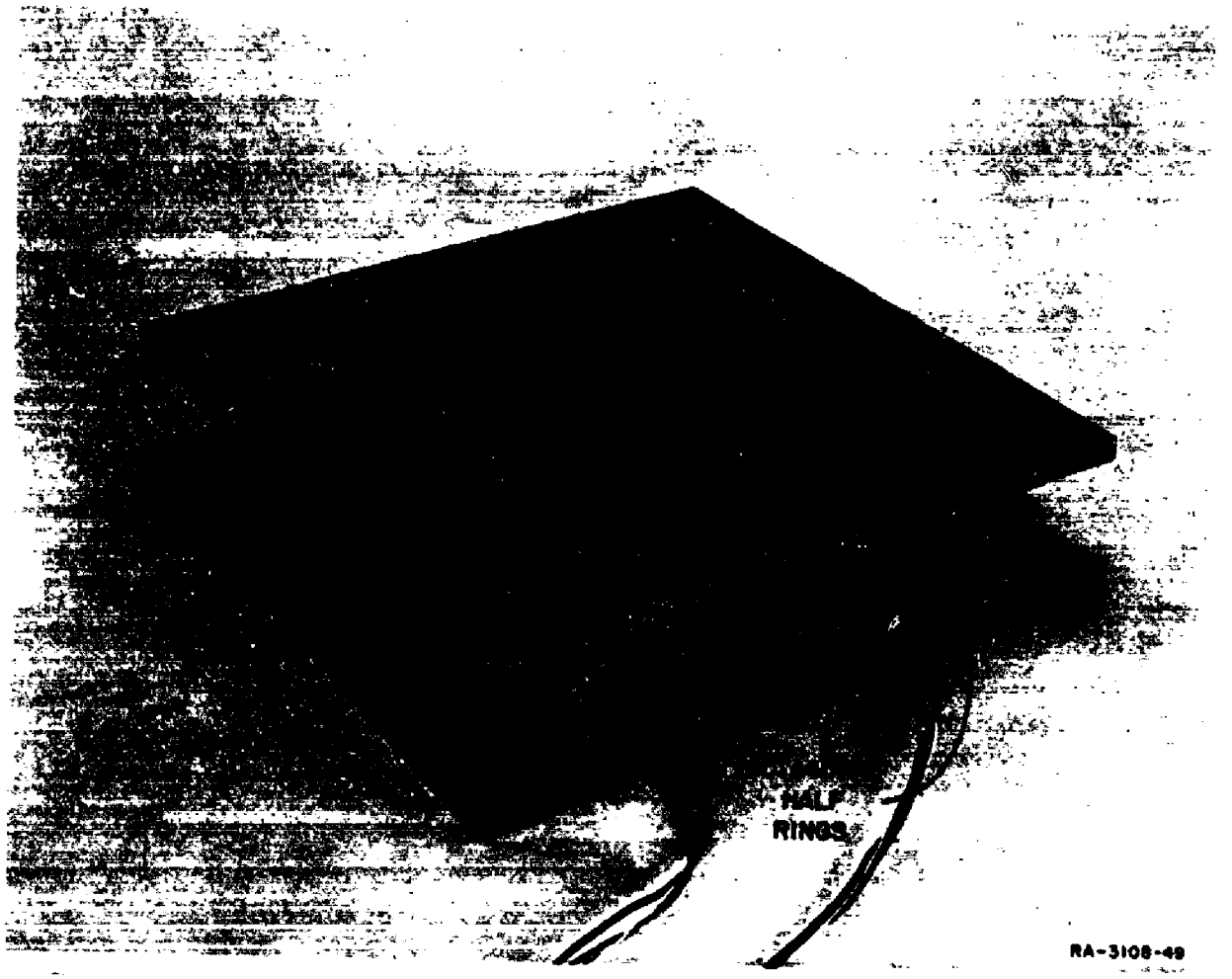

FIG. 8 SURFACE SHEAR GAGE

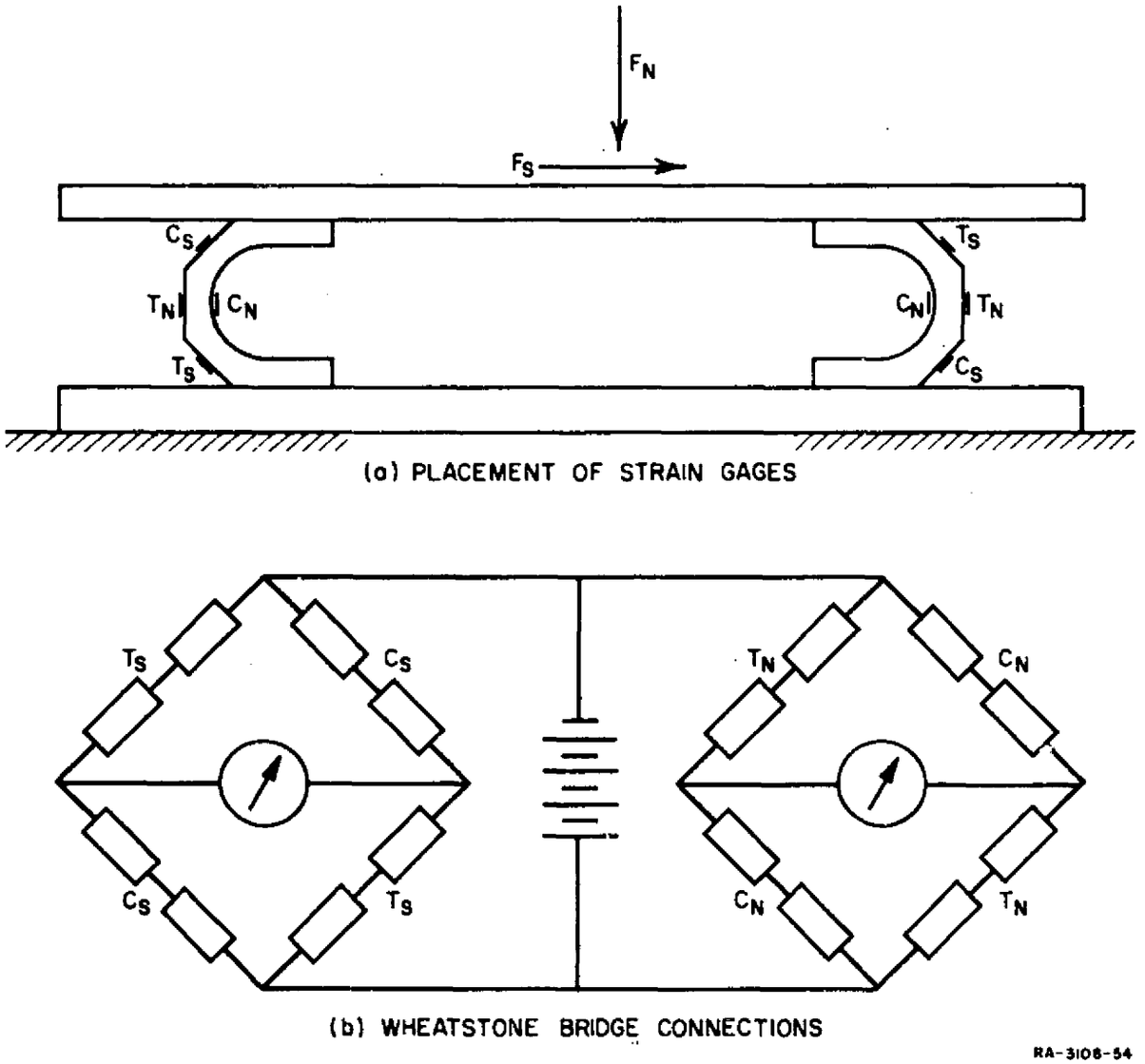

FIG. 9 SURFACE SHEAR GAGE INSTRUMENTATION: (a) PLACEMENT OF STRAIN GAGES, (b) WHEATSTONE BRIDGE CONNECTIONS

The type of measurement for which the shear gage is intended has not been attempted before and little is known about the magnitude of the shear stresses to be expected. However, it is known that the limit of transmissibility of shear stresses in soils is about 0.2 times the normal stress. Thus, 40 psi is probably a reasonable estimate of the maximum shear stress in the 200 psi overpressure region. 40 psi also sounds reasonable from the standpoint of dynamic pressure. The air phase dynamic pressure in the 200 psi overpressure region is about 325 psi. Therefore, the estimated 40 psi provides for a surface drag coefficient of about 0.1 referred to the air phase, plus a contribution from the suspended dust.

Design calculations for the shear gage are given in Appendix A. The present program was limited in scope to the design and fabrication of the gage itself and did not include plans or specifications for field use.

2. Calibration

The calibration curves for the surface shear gage are shown in Fig. 10 where strain is plotted as a function of applied force. The design shear stress of 40 psi is equivalent to an applied force of 5760 lbf while the design normal stress of 200 psi is equivalent to an applied force of 28,800 lbf.

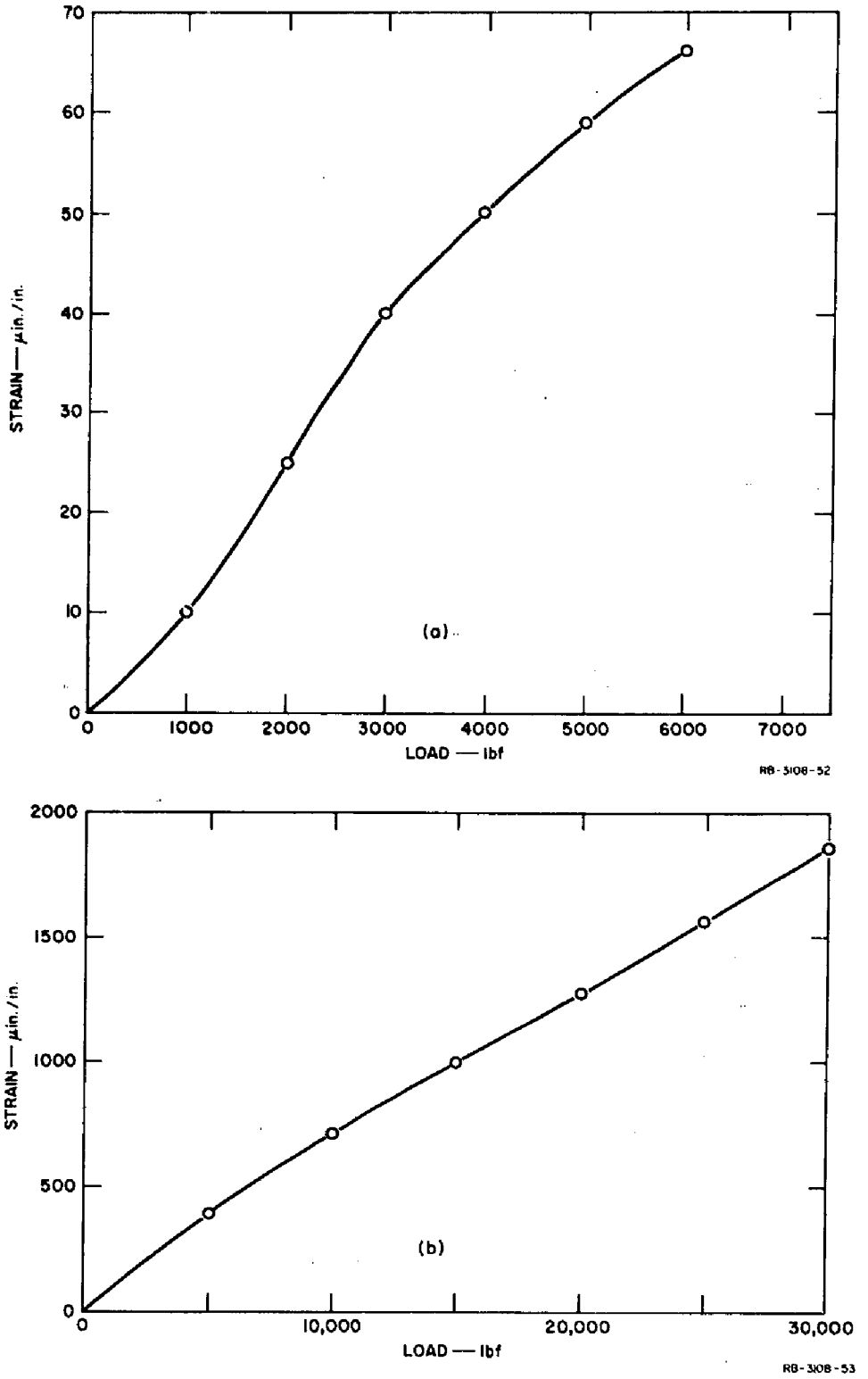

FIG. 10 SURFACE SHEAR GAGE CALIBRATION: (a) RESPONSE TO SHEAR LOADS, (b) RESPONSE TO NORMAL LOADS

IV DISCUSSION

The results of the track tests were disappointing and questions about the MAD gages' behavior remain unanswered. Due to shortcomings in telemetry and in the simulation of dust loading, dust response data were inconclusive, neither proving nor disproving the validity of the analog solution. From the clean air data it is evident that the gages are not sensing true static pressure.

Unfortunately, the tests were condensed into a short period of time at the end of the program and velocity data were not available in time to take remedial action. It is probable that the problem of sensing static pressure correctly could have been resolved had some of the tests been directed toward that objective.

When the telemetry and dust loading problems were recognized every effort was made to improve performance, but there seemed no reasonable alternative to continuing the tests as planned, once the expense of preparing for them had been borne.* It seemed unlikely that a practical method could be developed whereby dust loading at supersonic velocities could be simulated in the laboratory and calibration in our subsonic "dusty" wind tunnel would be meaningless.

Although the scope of this program did not include plans or specifications for deployment of the instruments in the field it was necessary to visualize their field mountings in order to arrive at practical configurations. The MAD gages, total drag probes, and dust samplers can be conveniently mounted on the same kind of towers that have been used at the Nevada Test Site in previous tests.

---

* In planning the track test program a sled borne tape recorder system was rejected in favor of telemetry because the "pre-record-erase" method of recording used at AFMDC did not have a satisfactory frequency response. Had the telemetry problem been anticipated at the outset it is probable that a satisfactory direct-record system could have been developed.

The surface shear gage can be deployed in several basically different ways. For example, the shear plate of the gage may be covered or uncovered, and, if covered, may be isolated from the surrounding soil or made an integral part of it. There is also the question of whether the gage should have its bottom surface fastened to a solid foundation or simply be imbedded in the soil.

At present we favor a solid mounting with the shear plate isolated from the surrounding soil and with a shallow covering of soil perhaps 2- to 4-inches-thick. Therefore, the gage was designed for (but is certainly not restricted to) being bolted down solidly.

Tentative plans call for the gage to be mounted on a concrete base surrounded by concrete walls to a height even with the top of the shear plate. The shear plate, the walls, and the surrounding area will then be covered with a layer of soil of appropriate depth. A soft rubber membrane will be installed between the shear plate and the surrounding concrete walls to exclude soil during the preparation of the surface. Depending on the nature of the soil layer, it may be possible to provide a small air gap between the soil directly over the shear gage and the surrounding soil. This could be accomplished by a removable framework placed over the gage while compacting the soil.

The prediction of a 40 psi shear stress for this gage in the 200 psi overpressure region is certainly doubtable and must be considered as a first approximation. However, the gage can withstand over five times the design shear stress without exceeding elastic limits while the least count of the gage in shear is about 1% of the design.

The proper operation of the dust samplers depends almost entirely on the precision timing of the closure devices and these have been extensively tested and used successfully in the field. It will be necessary to develop a triggering circuit that will initiate the closures at the proper time. It is our feeling that the firing signal can be initiated by the advancing shock wave through a pressure switch. Information on shock patterns ahead of cylindrical tubes is readily available in the literature (see Ref. 5).

APPENDIX A

DESIGN CALCULATIONS

APPENDIX A

DESIGN CALCULATIONS

MAD Gages

Except for a sharpening of the nose section to minimize the shock detachment distance, and an increase in the effective length of the pitot tube, the critical dimensions of the MAD gages are very nearly the same as those of the probe developed previously for subsonic flow.

The pitot tube I.D. is 0.093-inch compared to 0.096-inch in the previous design and the vent-to-tube area ratio is 5.7 compared to 5.8. The effective length of the pitot tubes in the current gages is approximately 6.5 inches compared to 6 inches previously. The major diameter of the gages is 1.75 inches and their cantilevered lengths, that is, the distance from nose tip to forward extremity of mounting bracket, are roughly 7-1/2 inches for gages A, B, C, and 8-1/2 inches for gage D.

Assuming as the limiting case that the Mach number of the flow out the vent is unity, the Mach number of the flow through the tube is then, from Ref. 5, approximately 0.1 and the pressure inside the tube is approximately 0.993 P_0 where P_0 is the total pressure of the air phase in the free stream. Thus, the error introduced by venting is at all times less than 1% of dynamic pressure.

The pressure transducers used in the MAD gages are dual coil, variable reluctance, diaphragm type, Ultradyne Model S-30. Standard pressure ranges are used, selected on the basis of the operating conditions shown in Table I (Ch. III) and assuming a maximum dust registry coefficient, N, of 0.75 for the rear port. The appropriate values are tabulated in Table A.1. The transducers in gages A and B will withstand 200% of full range pressure and the other transducers will withstand 150% of full range pressure without effect on their calibration.

The time response to air phase dynamic pressure with air as the pressure medium in all pressure passages is about 10 milliseconds. This response was measured by applying pressure to the probe through the front inlet and suddenly releasing the pressure by rupturing a mylar diaphragm.

Table A.1

PRESSURE RANGES FOR MAD GAGE TRANSDUCERS*

Gage No.	Design Overpressure (psi)	q_a (psi)	$N\phi_d$ (psi)	Transducer Pressure Ranges (psi)	
				Forward	Rear
A	50	32	72	0 - 75	0 - 75
B	100	112	252	0 - 150	0 - 300
C	200	308	692	0 - 750	0 - 1000
D	500	1075	2420	0 - 2000	0 - 3000

The time response to dust momentum flux cannot be measured conveniently since a pressure differential between two points in an open tube is required. However, on the basis of relative volumes, the time response to dust is estimated to be between 4 and 5 milliseconds. There is opportunity for improving the response time to both air and dust, perhaps by a factor of two, by partially filling the pressure passages with an incompressible fluid.

Total Drag Probe

Design Loads. Refer to Table I (Ch. III) for dynamic pressures and compute the drag force, F_D, for each probe. In Table A.2,

$$F_D = C_D A q_{tot} \qquad (A.1)$$

where

C_D = 1.0 by assumption

A = 3 x 3 = 9 in.^{2} (projected target area)

$q_{tot} = q_{air} + \phi_d$ (from Table I)

*Nomenclature definitions are listed on a fold-out page at the end of this report.

Table A.2

TOTAL DRAG PROBE DESIGN LOADS

Probe No.	Design Overpressure (psi)	q_{tot} (psi)	F_D (lbf)	W_{max} (lb/in.)	M_{max} (in.-lb)	h (in.)
A	50	128	1150	180	32.1	0.0878
B	100	448	4030	630	112.3	0.165
C	200	1232	11100	1750	312	0.1634
D	500	4300	38700	6000	1070	0.250

Mounting Cylinder

Consider the mounting cylinder as a 3-inch-diameter beam cantilevered from point of attachment 2-1/2 diameters (7.5 inches) from the center of the probe.

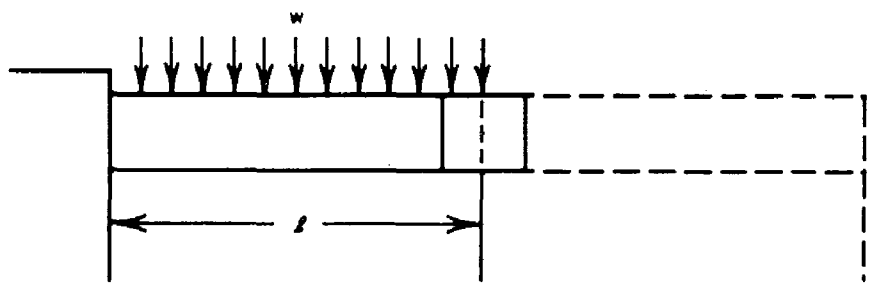

ℓ = 7.5 in.

$z = \frac{I}{c}$ = 2.651 $in.^3$

$w = 3q_{tot}$

RA-3108-59R

Then,

$$\sigma_{max} = \frac{\omega \ell^2}{2Z} = \frac{3q_{tot} \times 7.5^2}{2 \times 2.651} = 31.8\ q_{tot} \qquad (A.2)$$

For a factor of safety of 1.8, use materials with working stress, σ, as follows:

$\sigma = 1.8 \times 31.8 \times 125 = 7150$ psi for probe A

$\sigma = 1.8 \times 31.8 \times 448 = 25700$ psi for probe B

$\sigma = 1.8 \times 31.8 \times 1232 = 70500$ psi for probe C

$\sigma = 1.8 \times 31.8 \times 4300 = 246000$ psi for probe D

Target Cylinders

Make all cylinders 2-1/2-inch I.D. with a nominal 3-inch O.D. For maximum bending stress consider the cantilevered section from the 25° point to have a triangular load distribution diagram varying from W_{max} at the 25° point of support to 0 at the point of interference with the fixed portion. W_{max} was chosen conservatively high so the load distribution diagram to be expected from a cylinder in cross-flow was entirely enclosed in the triangular load diagram (see Ref. 6).

Then, from Ref. 7,

$$M_{max} = \frac{s^2 W_{max}}{15} = \frac{1.635^2 W_{max}}{15} = 0.178\ W_{max} \qquad (A.3)$$

$$\sigma = \frac{MC}{I} = \frac{6M}{bh^2} \quad , \text{ or} \qquad (A.4)$$

$$h = \sqrt{\frac{6M_{max}}{\sigma}} \qquad (A.5)$$

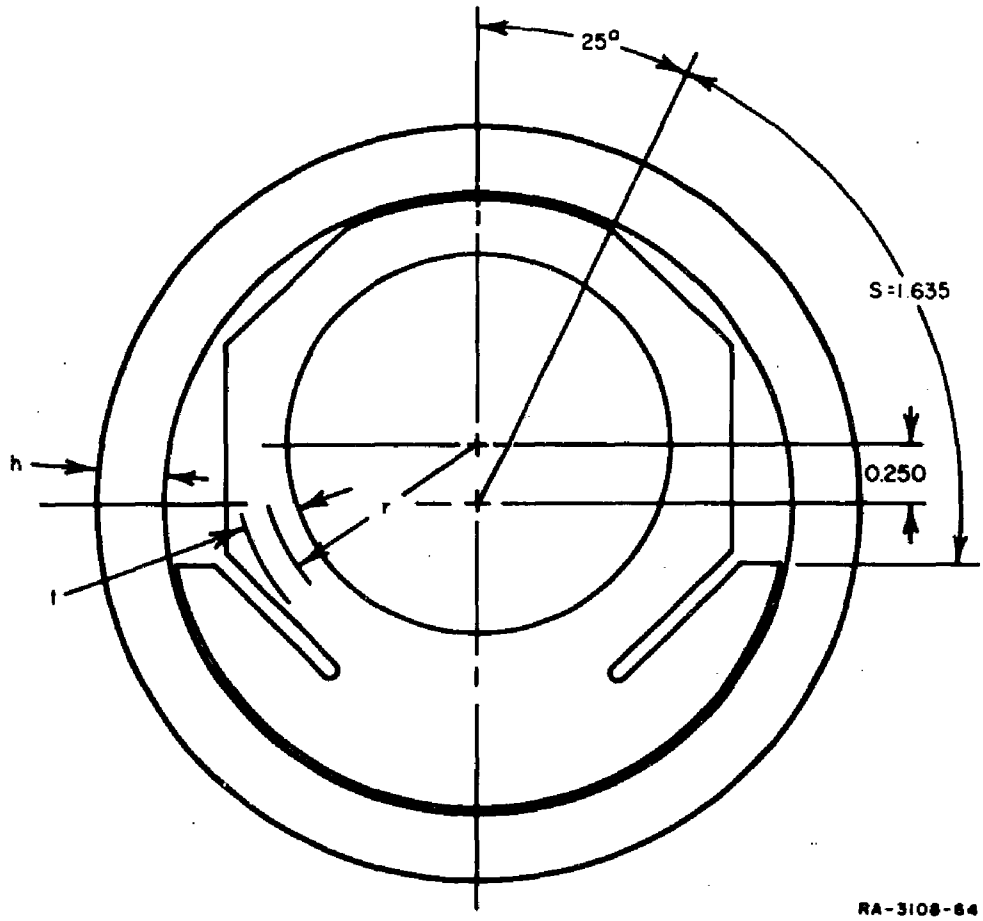

These design parameters are tabulated in Table A.2. Target cylinders A and B and octagonal rings A, B, and C were made from 2024-T4 aluminum with a working stress of 25000 psi. Target cylinders C and D and ring D were made from 4140 steel and heat treated to the calculated strength.

Octagonal Proving Rings

From Ref. 8,

$$\sigma = \frac{1.09\ F_D\ r}{b t^2} \qquad (A.6)$$

$$K = \frac{2.5\ E\ bt^3}{1.8\ r^3} \tag{A.7}$$

$$\delta = \frac{F_D}{K} \tag{A.8}$$

$$\epsilon = \frac{\sigma}{E} \tag{A.9}$$

where

σ = stress at the point of strain measurement

F_D = total drag force (Table A.2)

b = three inches for all gages

δ = deflection at design load, F_D

ϵ = strain at the point of measurement

For aluminum (gages A, B, and C), $E = 10 \times 10^6$ psi. For steel (gage D), $E = 30 \times 10^6$ psi.

$$f_N \simeq \frac{1}{2\pi} \sqrt{\frac{K}{m}} \tag{A.10}$$

where

f_N = natural frequency of the system

m = mass of the target cylinder, plus one-half of the mass of the octagonal ring

To estimate the error, ΔF, in drag measurement due to acceleration of the supporting structure, assume a maximum ground mass acceleration, a_g, of 10 g. Then,

$$\Delta F = \frac{m_{cyl}}{g_c} \times a_g = 10\ m \tag{A.11}$$

or

$$\frac{\Delta F}{F_D} = \frac{10\ m}{F_D} \tag{A.12}$$

Table A.3

DESIGN PARAMETERS, TOTAL DRAG PROBES

Probe No.	F_D (lbf)	r (in.)	t (in.)	(psi)	K (lbf/in.)	δ (in.)	ϵ (μ in./in.)	m (lbm)	f_N (cps)	$\Delta F/F_d$
A	1,150	0.875	0.25	5,850	967×10^3	0.0012	585	0.555	4130	0.0048
B	4,030	0.875	0.25	20,500	967×10^3	0.0042	2,050	0.555	4130	0.00137
C	11,100	0.819	0.362	25,000	3600×10^3	0.0031	2,500	1.470	4900	0.00132
D	38,700	0.828	0.344	98,500	8960×10^3	0.0043	3,280	2.596	5800	0.00067

Dust Sampler

The dust sampler tubes were made to conform with specifications for an existing tube-closure system (Ref. 9). The tubes are 36-inches-long, 2-inches I.D., and have 1/4-inch-thick walls. Material is 1010-1020 annealed steel tubing (Shelby seamless). The walls at the leading ends of the tubes are tapered to a 15° wedge to permit the attachment of an oblique shock wave around the periphery (Ref. 5). "Pillow block" type clamps are provided at two points along the tube's length, one 12 inches aft of the leading end and one 12 inches forward of the trailing end. Grooves are provided at the points of attachment to enable the clamps to resist axial thrust of the tube (see Fig. 7). Two small bleed holes are provided under each clamp to permit venting before the tubes are opened for analyses.

Each of the two explosive closures in a dust sampler involves a detonator, a high explosive charge, and the containing hardware. When a signal is fed simultaneously to the two detonators, the initiation of the closure can be controlled to within $\pm$ 0.25 microseconds, and the completion of the closure to within $\pm$ 1 to 2 microseconds depending on the selection of the high explosive charge, i.e., whether the two charges were taken from the same batch. The time required for closure is about 30 microseconds.

Surface Shear Gage Design

Design Loads

The surface shear gage was designed for the 200 psi overpressure region and the surface area of the gage is 1-ft^2. Therefore, the design normal force, F_N, is

$$F_N = 200 \times 144 = 28,800 \text{ lbf} \qquad (A.13)$$

As a first approximation it was assumed that the maximum shear stress, F_S, in the 200 psi region would be 40 psi (see discussion, Ch. III). Thus, the total design shear force is

$$F_S = 40 \times 144 = 5,760 \text{ lbf} \qquad (A.14)$$

The feasibility of using an aluminum honeycomb sandwich structure was investigated but the complexities in mounting and attachment of components more than offset the savings in weight. Therefore, a solid aluminum plate was used as the load bearing surface.

Shear Plate Design

Consider as a simply supported beam of unit width and $\ell = 2.828\ a$ (for optimum support).

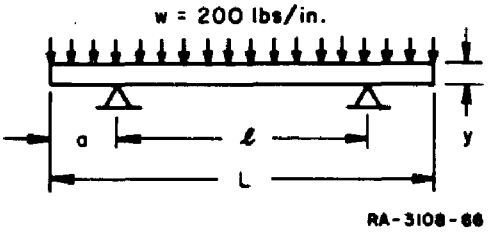

Then, from Ref. 7,

$$\sigma = \frac{wL^2}{46.62\ Z} \qquad (A.15)$$

L = 12-inches

$\ell = 2.828\ a$

$Z = \frac{I}{c} = \frac{y^2}{6}$

or

$$Z = \frac{wL^2}{46.62\ \sigma}$$

For 6061-T6 aluminum with a working stress of 25,000 psi,

$$Z = \frac{200 \times 12^2}{46.62 \times 25{,}000} = 0.024$$

$$y = \sqrt{6Z} = 0.38\ , \quad \text{say } y = 3/8 \text{ inch}$$

Octagonal Ring Design

From Ref. 9, considering the two half rings as one full ring,

$$\sigma = \frac{1.09\ F'_N r}{bt^2} \tag{A.17}$$

where, for a unit width beam, $b = 1.0$, and $F'_N = 200 \times 12 = 2400$

or

$$t^2 = \frac{1.09\ F'_N r}{b\sigma} \tag{A.18}$$

Assume 2024-T4 aluminum with a working stress of 25,000 psi and try $r = 1$ inch for a first approximation. Then,

$$t = \sqrt{\frac{1.09 \times 2400}{25{,}000}} = 0.324$$

Adjusting to $r = 0.85$, trying for an even 2-inch height,

$$t = \sqrt{\frac{1.09 \times 2400 \times 0.85}{25{,}000}} = 0.298\ , \quad \text{say } t = 0.300 \text{ inch}$$

Horizontal Strain

From Ref. 9,

$$\epsilon = \frac{2.18\ F'_s r}{Ebt^2} \tag{A.19}$$

where

$F_s' = 40 \times 12 = 480$ (for a unit width beam)

$r = 0.85$

$b = 1$

$t = 0.3$

$E = 10 \times 10^6$

$$\epsilon = \frac{2.18 \times 480 \times 0.85}{10^7 \times 1 \times 0.09} = 0.00099 \text{ inch.}$$

Stiffness in Shear and Natural Frequency

From Ref. 9,

$$K_s = \frac{2.5\ Ebt^3}{3.6\ r^3} = \frac{2.5 \times 10^7 \times 0.3^3}{3.6 \times 0.85^3} = 306 \times 10^3 \text{ lbf/in.} \qquad (A.20)$$

The natural frequency, f_N, neglecting the mass contribution from the octagonal rings and the soil is

$$f_N = \frac{1}{2\pi} \sqrt{\frac{K}{m}} \qquad \text{where } m = 0.45 \text{ lbm/unit width} \qquad (A.21)$$

$$= \frac{1}{2\pi} \sqrt{\frac{30.6 \times 10^4 \times 386}{0.45}} = 2580 \text{ cps}$$

Ground Acceleration Error

Assuming the ground mass acceleration, a_g, does not exceed 10 g the error in shear measurement, ΔF_s, is

$$\Delta F_s \leq \frac{M}{g_c} a_g \qquad (A.22)$$

where

$M = 12\ m = 5.4$ lbm

$F_s = 12\ F_s' = 5760$ lbf

and

$$\frac{\Delta F_s}{F_s} \leq \frac{M\ a_g}{g_c\ F_s} = \frac{5.4 \times 322}{32.2 \times 5760} = 0.0094 \qquad (A.23)$$

APPENDIX B

ANALOG SOLUTION FOR MAD GAGE

APPENDIX B

ANALOG SOLUTION FOR MAD GAGE

The general problem of predicting dust registry coefficients for the MAD gages was handled on a Model 2100 Donner analog computer and tests were conducted on a supersonic rocket sled track to check particular solutions.

To make the problem tractable several simplifying assumptions are necessary. The general assumptions used for the analog computer solution are:

(1) The dust and air are in velocity equilibrium in the free stream.

(2) The air flow pattern is not affected by the presence of dust.

(3) The air behind the shock decelerates isentropically.

(4) The dust particles behave as individual spheres without interaction and decelerate due to drag forces alone.

(5) The dust is distributed uniformly and the particle diameters are very much smaller than the probe entrance diameter.

(6) All dust particles entering the probe exit at velocities greater than or equal to the velocity of the aspirating air.

(7) The capture efficiency of the probe is unity for all particle sizes of interest.

(8) Heat transfer effects are negligible.

(9) All particle momentum loss is recovered as a pressure rise within the tube.

(10) The velocity of the dust particles will not decrease substantially in going through the shock wave.

Assumptions (2) and (4) imply that the dust concentration will not be too high. At high dust concentrations the particles will interfere with each other and influence the airflow pattern. Although it is difficult to define a "high" dust concentration with assurance, it should be realized that even with a mass ratio (dust to air) of unity the dust particles occupy less than 1/10 of 1% of the total volume occupied by the mixture.

Assumption (8) tends to make the computed deceleration rate less than the actual rate. The air temperature increases upon crossing the shock wave while the particle temperature, because of thermal lag, requires a finite time to reach equilibrium. Therefore, the particles will be receiving heat from the air resulting in a decrease in air temperature and viscosity of the air and an increase in air density. If these effects were taken into account, the computed drag would be larger. However, the error is not expected to be large because of the very short transit time and the low heat transfer coefficient between particles and air.

As a consequence of assumption (1), we may consider the pressure rise due to dust momentum transfer independent of the air phase.

Referring to the diagram and using the momentum law,

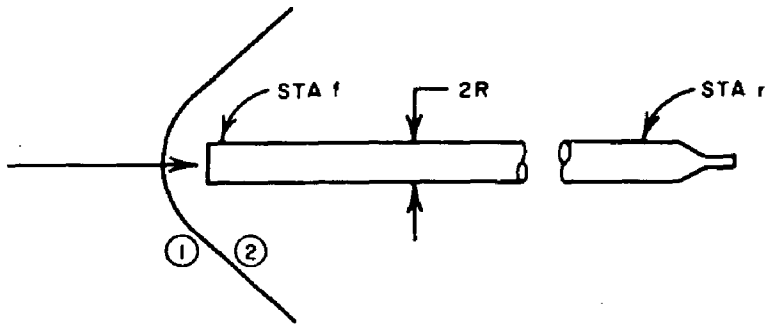

then,

$$(P_{fm} - P_{fo}) = \frac{w}{Ag_c} v_2 - \sum \frac{1}{n} \frac{1}{g_c} \left(\frac{w}{A}\right)_i v_{fi} \qquad (B.1)$$

where

P_{fm} = pressure at the front port for the mixture (psi)

P_{fo} = pressure at the front port for clean air (psi)

w = mass flow rate of dust (lb/sec)

A = cross sectional area of the tube (in.^{2})

v = dust particle velocity (ft/sec)

Subscript i refers to a particle of a particular diameter. The first term on the right of Eq. (B.1) is the momentum flux per unit area directly behind the shock. The second term is a summation of the dust momentum flux at f.

From assumptions (1) and (10), Eq. (B.1) becomes

$$g_c (P_{fm} - P_{fo}) = \frac{w}{A} V_1 - \sum_n \left(\frac{w}{A}\right)_i v_{fi} \tag{B.2}$$

and for a dust composed of particles of uniform size Eq. (B.21) becomes

$$g_c (P_{fm} - P_{fo}) = \frac{w}{A} (V_1 - v_f) \tag{B.3}$$

Equations (B.1), (B.2), and (B.3) apply to the rear port if we replace subscript f with subscript r.

The efficacy of the MAD gage may be expressed in terms of a dust registry coefficient, N, which is defined as the ratio of air phase pressure rise to total dust momentum flux. From Eq. (B.3) for dust of uniform size,

$$N_f = \frac{V_1 - v_f}{V_1} \tag{B.4}$$

and

$$N_r = \frac{V_1 - v_r}{V_1} \tag{B.5}$$

Ideally, $N_f = 0$ and $N_r = 1$ which means that the front port measures air dynamic pressure only and that the rear port measures all the dust momentum flux.

To compute particle velocity we apply Newton's second law to a particle in motion, i.e.,

$$4/3\ \pi\ \rho_d\ a^3\ \frac{dv}{dt} = -\ \pi\ a^2\ C_D\ \frac{\rho_a}{2}\ (v - V)^2 \tag{B.6}$$

where

ρ_d = dust particle density (lb/ft^3)

$2a$ = dust particle diameter (ft)

v = dust particle velocity (ft/sec)

t = time (sec)

C_D = drag coefficient

ρ_a = air density (lb/ft^3)

V = local air velocity (ft/sec)

Equation (B.6) becomes

$$\frac{d\bar{v}}{d\tau} = - \frac{C_D}{24} N_R (\bar{v} - \bar{V}) \qquad (B.7)$$

with boundary condition, $\bar{v} = 1$ at $\tau = 0$ (B.8)

where we define

$$\bar{v} = \frac{v}{V_1}$$

$$\bar{V} = \frac{V}{V_1}$$

and N_R = Reynolds number = $(\bar{v} - \bar{V}) \frac{2a}{\mu_a} \rho_a$ (with the air density taken as the average between conditions just behind the shock and at the mouth of the probe)

$$\tau = \frac{V_1 t}{\lambda_s}$$

where λ_s = Stoke's law stopping distance = $\frac{2}{9} \left(\frac{\rho_d a^2 V_1}{\mu_a} \right)$.

Equation (B.7) is nonlinear since both C_D and N_R are functions of the relative velocity $(\bar{v} - \bar{V})$ and a closed form solution is not apparent.

Substituting the nondimensional velocities in Eqs. (B.4) and (B.5), we write

$$N_f = 1 - \bar{v}_f \qquad (B.9)$$

and

$$N_r = 1 - \bar{v}_r \qquad (B.10)$$

Particle velocities were computed from Eqs. (B.7) and (B.8) using a Model 3100 Donner analog computer. The program is described in Fig. B.1. The computed velocities were then used in Eqs. (B.9) and (B.10) to determine the theoretical dust registry coefficients, front and rear. Particular solutions were obtained for the following range of variables:

ρ_d = 170 (lb/ft^3) (chalk dust)

2_a = 4, 20, 40 (microns)

M_1 = 1.25, 1.47

T_1 = 530 (^{0}R)

P_1 = 14.7 (psi)

The air velocity is assumed to decay linearly from $\bar{V}_2$ just behind the shock to the aspirating velocity, 0.2 $\bar{V}_2$, at the mouth of the probe. An aspirating velocity of 0.2 $\bar{V}_2$ means that the maximum N_r is 1 - 0.02 $\bar{V}_2$

$$\bar{V} = \bar{V}_2 \, [0.2 + 0.8 \, (1 - \bar{\chi})] \tag{B.11}$$

The new variables are defined as

$$\bar{V}_2 = \frac{V_2}{V_1}$$

$$\bar{x} = \frac{x}{\ell}$$

where

x = distance from the shock wave

ℓ = shock detachment distance

The drag coefficient was considered to be a function of both Mach and Reynolds numbers. For Mach numbers greater than 0.3, data from Ref. 10 were used; for Mach numbers less than 0.3 incompressible data were used.

The viscosity was computed from the Sutherland type equation,

$$\mu = \frac{3.27 \times 10^{-7} \, (5T - 3)}{1 + \frac{1008}{5T - 3}} \left(\frac{\text{lb}}{\text{ft-sec}}\right) \tag{b.12}$$

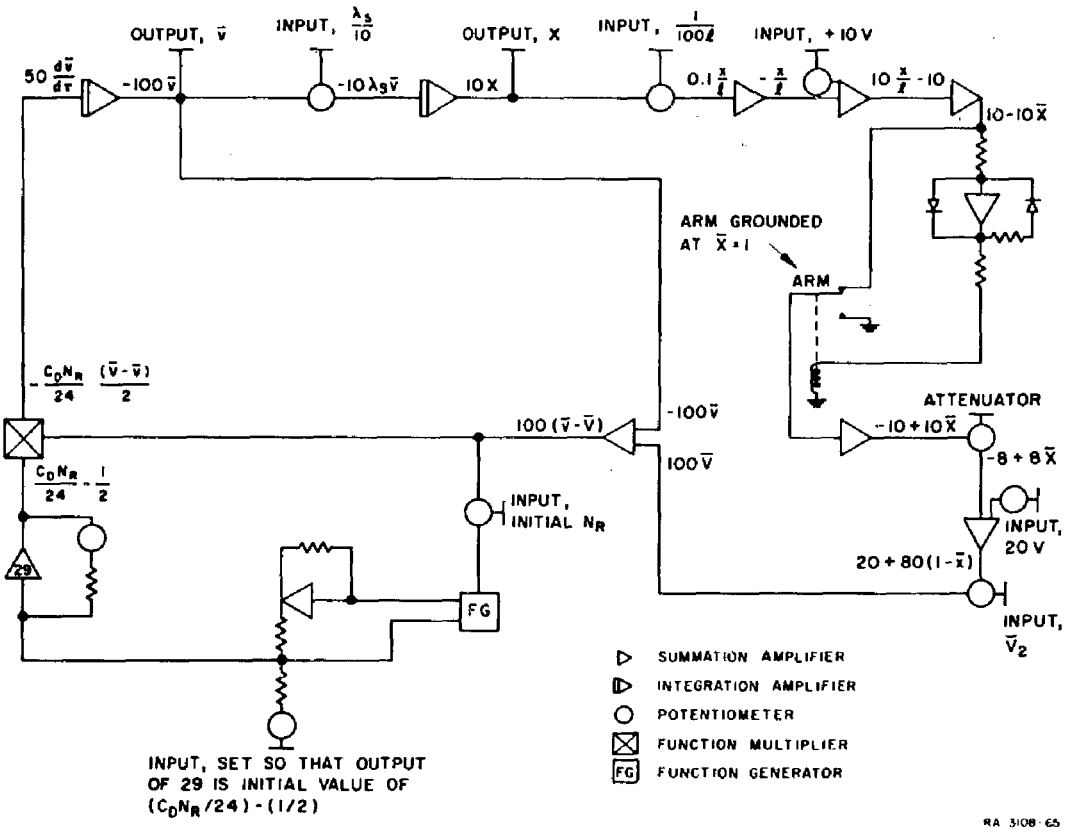

FIG. B.1 ANALOG COMPUTER PROGRAM

where T is the temperature in degrees Rankine taken as the average between the conditions behind the shock wave and at the mouth of the probe.

The dust registry coefficients computed from Eq. (B.7) for three particle sizes and for two velocities are tabulated in Table B.1.

Table B.1

COMPUTATION OF DUST REGISTRY COEFFICIENTS

Mach No.	V_1 (fps)	2a (μ)	N_f	N_r
1.25	1400	40	0.052	0.750
		20	0.243	0.837
		4	0.86	0.86
1.47	1660	40	0.034	0.668
		20	0.295	0.875
		4	0.89	0.89

APPENDIX C

ROCKET SLED TESTS

APPENDIX C

ROCKET SLED TESTS

Summary and Conclusions

The test program was undertaken in the absence of a suitable laboratory facility to check the analog solution for dust registry coefficients and to test the behavior of the gages as supersonic pitot tubes in clean air.

Due to the inadequacies in the telemetry system and in the creation of dust momentum flux no conclusive data on dust registry coefficients were obtained. This was the first time a telemetry system had been used in a small monorail sled and the high vibration environment together with the low profile resulted in unsteady signal transmission. The records indicate that the time response of the gages was satisfactory but the information recorded during the very short interval of dust loading—about 5-1/2 milliseconds at the 1600 ft/sec station and 7-1/2 milliseconds at the 1200 ft/sec station—was invariably obscured by noise. To obtain meaningful data it would have been necessary to sustain dust loading for tenths of seconds rather than milliseconds. Furthermore, it was much more difficult to create heavy dust clouds than was anticipated and dust loading was much lower than planned.

For the clean air portion of the runs the data, though difficult to interpret accurately, leave no doubt that the dynamic pressure measurements are consistently low and that the ratio of measured dynamic pressure to actual dynamic pressure is not constant with velocity. The clean air behavior of gages A and B is shown in Table C.1 and in Fig. 4. The ratios of gage pressure to actual pressure and the mean values and standard deviations are based on the results of eight tests. The records from gage C, the least sensitive of the three gages, were in general too noisy to yield reliable data.

The gages were checked before each run and there was no evidence of plugging; shadowgraph photos taken at different stations indicated that the air stream was undisturbed ahead of the probes. Therefore, the only

Table C.1

MAD GAGE CLEAN AIR RESPONSE

Sled Velocity (fps)	q_{ideal} (psi)	Gage Response, $\frac{q_{gage}}{q_{ideal}}$			
		GAGE A		GAGE B	
		Mean	Standard Deviation	Mean	Standard Deviation
2050	46.2	0.723	0.0321	0.738	0.0305
2000	43.6	0.733	0.0651	0.701	0.1415
1950	41.1	0.732	0.0816	0.715	0.1226
1900	38.9	0.708	0.0619	0.684	0.0976
1850	36.5	0.710	0.0771	0.679	0.1158
1800	34.2	0.690	0.0951	0.684	0.1156
1750	32.2	0.684	0.0906	0.703	0.0322
1700	30.0	0.655	0.0926	0.660	0.0461
1650	27.9	0.653	0.1008	0.629	0.0758
1600	26.1	0.593	0.0857	0.632	0.0898
1550	24.2	0.595	0.1158	0.599	0.1019
1500	22.2	0.569	0.1248	0.600	0.1113
1450	20.4	0.550	0.1098	0.601	0.1451
1400	18.7	0.516	0.1462	0.588	0.1754
1350	17.2	0.480	0.1202	0.614	0.1861
1300	15.6	0.455	0.1460	0.708	0.1848
1250	14.1	0.472	0.0921	0.712	0.1862
1200	12.8	0.421	0.1458	0.618	0.2055
1150	11.5	0.424	0.1197	0.642	0.2055

explanation for the low dynamic pressure measurements is that the static pressure is not being sensed correctly. Shadowgraph pictures indicate that the flow is again supersonic before reaching the mounting plate but this does not mean, necessarily, that free stream conditions obtain at the static pressure ports. It is unfortunate that the track tests were run so late in the program and in such a short interval of time that velocity data were not obtained in time to change plans. Had the problem in static pressure measurement been recognized in the middle of the test series it may have been resolved in subsequent runs.

Test Plans

The voltage controlled sub-carrier oscillators in the telemetry system were not directly compatible with the variable reluctance transducers in the MAD gages. Therefore, a miniaturized signal conditioner package was designed and built by SRI. It provides 3-KC excitation for the Ultradyne transducers, an AC voltage amplifier and rectifier-doubler to give an output output of 0 to 5 volts. Calibration in the laboratory was accomplished by pressurizing the transducers directly and reading the voltage output from the signal conditioners. The calibration curves for the front and rear transducers in MAD gages A, B, and C are shown in Fig. C.1. The gain in the signal conditioners was adjustable within limitations. The calibration curves in Fig. C.1 represent the gage sensitivities for the major part of the test series. A 5-volt signal from the signal conditioner is equivalent to full band width for its sub-carrier oscillator. The magnitude of the pressures to be measured by the front transducer are shown in Table C.1 as q_{ideal}; the pressures to be measured by the rear transducer are shown in Table C.2 as Φ_d. Calibration steps with the sled in place before each run were provided by a pressure-resistance simulator box that produced the appropriate voltages at the output of the signal conditioners. The trackside calibration steps were transmitted to the receiving station and recorded on the tape.

During each test continuous velocity data were obtained by ribbon frame cameras. A typical space-time record is reproduced in Fig. C.2.

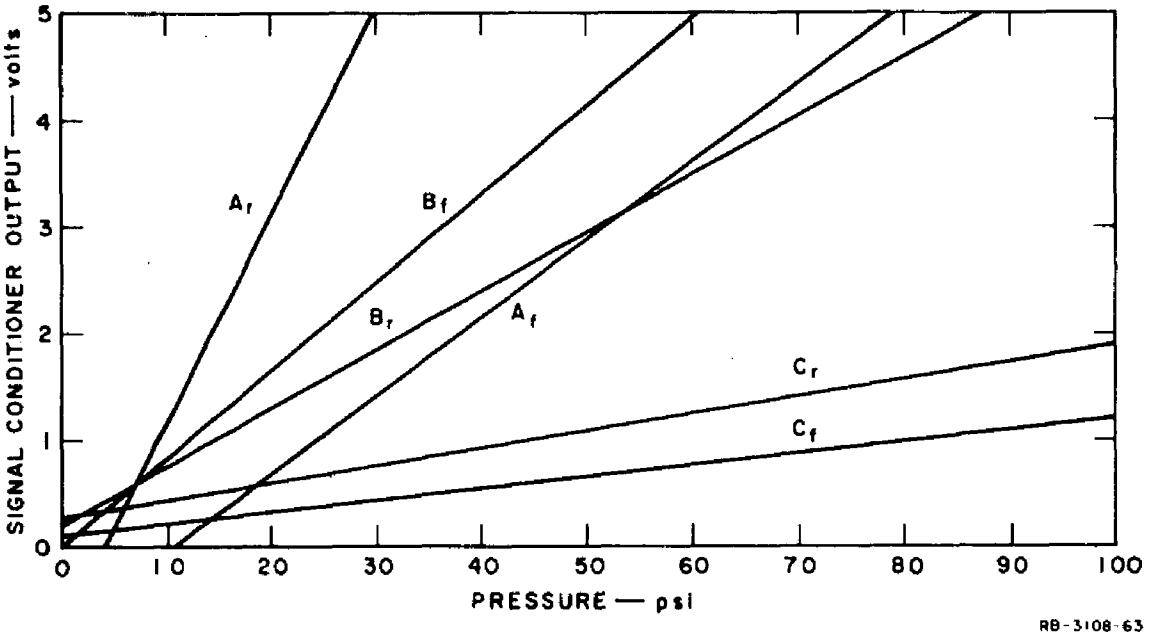

FIG. C.1 CALIBRATION OF MAD GAGES FOR TRACK TESTS

Dust blowers were placed at track stations where the appropriate velocities were expected to be reached in the coast phase of the sled's trajectory. Dust feeding was started automatically 2 seconds before time zero and continued until the dust was expended (about 14 seconds). The sled reached the dust in about 3-1/2 seconds when the generators were placed at the 1600 ft/sec station; the 1200 ft/sec station was reached in about 5 seconds. A log of the test series is shown in Table C.2.

Calculations

Clean Air Dynamic Pressure

Assume $T_{ave} = 545^{\circ}R$, $(P_s)_{ave} = 12.75$ psi (Ref. 11). Then, from Ref. 5,

$$c = 49.02\sqrt{545} = 1145 \text{ ft/sec} \qquad (C.1)$$

$$M = \frac{V}{c} = \frac{V}{1145} \qquad (C.2)$$

TABLE C.2

TRACK TEST CONDITIONS

DATE	Run No. SRI	Run No. AFMDC	Dust Station	Time to Dust (sec)	Velocity at Dust (ft/sec)	Type of Dust*	DUST LOADING m_d/ℓ	DUST LOADING W_d/W_a	DUST LOADING ξ_d (psi	Comments
5/15/63	1	45-2A	--	--	--	--	--	--	--	Instrumentation check-out. No dust loading attempted.
5/17/63	2	45-2B	--	--	--	--	--	--	--	Ditto. Re-adjusted sensitivities.
6/10/63	3	45-2C	--	--	--	--	--	--	--	Dust loading not attempted- excessive wind.
6/11/63	4	45-2D1	27600	5.30	1208	a	0.0885	0.212	2.2	
7/16/63	5	45-2H1	--	--	--	--	--	--	--	Dust loading abortive - compressor malfunction
7/17/63	6	45-2I1	--	--	--	--	--	--	--	Ditto
7/23/63	7	45-2J1	30220	3.36	1631	b	0.214	0.323	6.30	Modified dust generators to increase ξ_d**
7/23/63	8	45-2K1	30220	3.35	1644	c	0.322	0.497	9.55	
7/23/63	9	45-2L1	30220	3.33	1665	d	0.143	0.222	4.36	
7/24/63	10	45-2M1	27600	5.27	1216	b	0.322	0.497	5.22	
7/24/63	11	45-2N1	27600	5.21	1238	c	0.322	0.497	5.40	
7/24/63	12	45-2O1	27600	5.18	1249	d	0.230	0.356	3.94	
7/25/63	13	45-2P1	30220	3.35	1647	a	0.1785	0.276	5.32	

* a chalk dust, 4-40 μ
b glass beads, 18-40μ
c glass beads, 40-80 μ
d carbonyl iron, < 5 μ

** For Run No. 7 and subsequent runs, dust conveyor belt was above rather than below main duct. In this way capacity was increased and the system was less dependent on secondary compressor air.

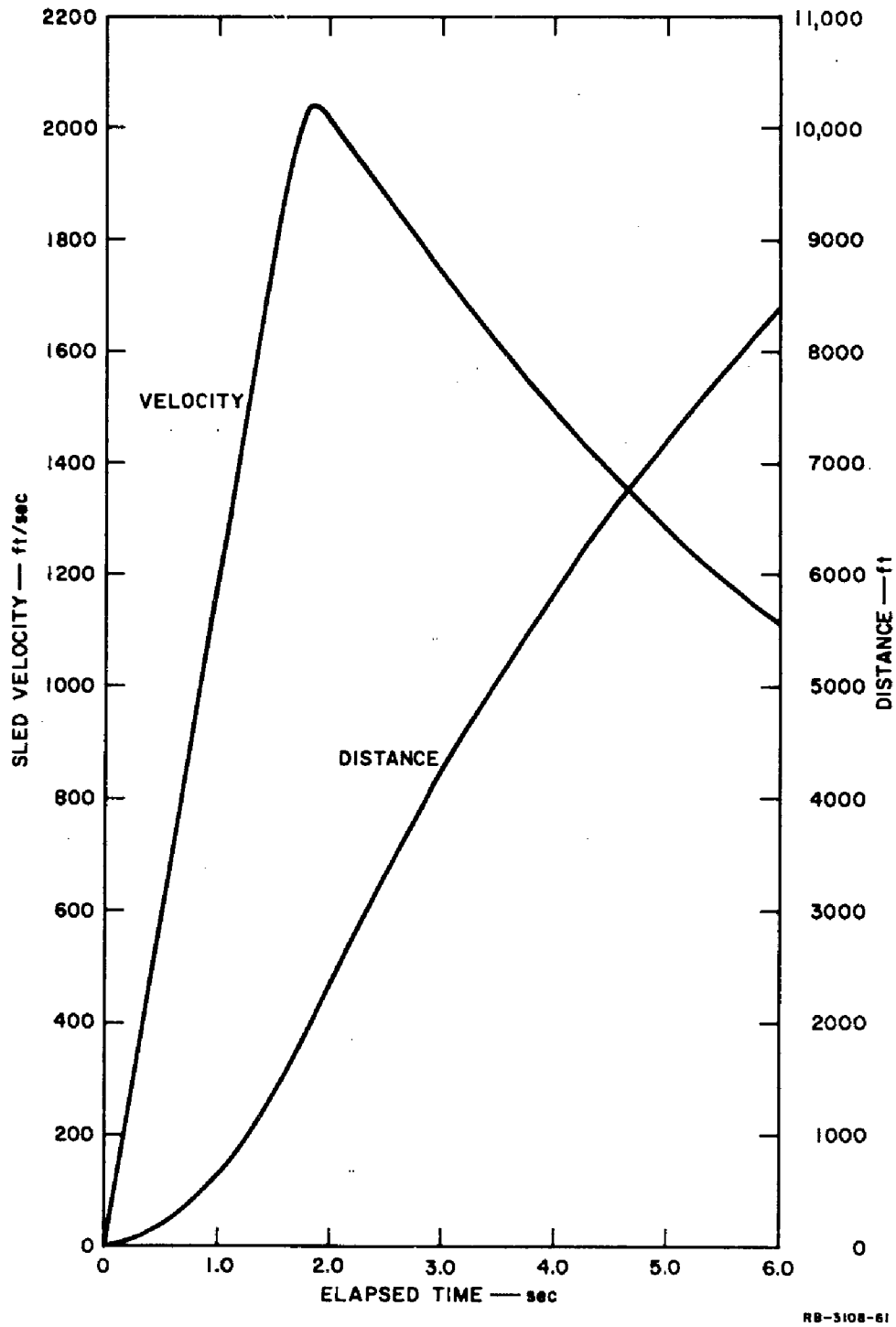

FIG. C.2 SPACE-TIME HISTORY FOR TYPICAL TRACK TEST

$$\frac{P_o}{P_s} = \varphi(M) \quad * \tag{C.3}$$

$$P_o = 12.75 \times \frac{P_o}{P_s} \tag{C.4}$$

$$q = P_o - P_s = 12.75 \left(\frac{P_o}{P_s} - 1 \right) \tag{C.5}$$

Dust Momentum Flux

The mass flow rate of air, w_a, through the dust generators was computed on the basis of the average velocity in the high velocity region. The average velocity was computed from pitot-static measurements at 42 points in the 1-inch x 36-inch duct.

$$w_a = \rho A V \tag{C.6}$$

where

ρ = air density

A = duct cross sectional area

V = average velocity

The mass flow rate of dust, w_d, was based on the average rate of dust addition.

$$w_d = \frac{m_d V_b}{\ell} \tag{C.7}$$

where m_d = net dust added to the system (i.e., the initial amount less any dust left in the duct)

V_b = dust conveyor belt velocity

ℓ = length of the dust layer

---

* Function φ is given in Ref. 5

$$\Phi_d = \frac{(\rho_m - \rho_a)\, V^2}{2\, g_c} \qquad (C.8)$$

where

V is now the sled velocity, and

ρ_m is the density of the mixture of air and dust in the dust cloud.

$$\rho_m = \frac{w_a + w_d}{Q_a + Q_d} \qquad (C.9)$$

or, since $Q_d \ll Q_a$

$$\rho_m \simeq \frac{w_a + w_d}{Q_a} = \frac{w_a + w_d}{w_a/\rho_a} = \rho_a \left(1 + \frac{w_d}{w_a}\right)$$

Thus,

$$\Phi_d = \rho_a \frac{w_d}{w_a} \frac{V^2}{2\, g_c} \qquad (C.10)$$

REFERENCES

1. Kriebel, A. R., Design and Calibration of a Total-Pressure Probe for Dust-Laden Air, Stanford Research Institute, Project SU 2534-2, Final Report, DASA-1158, July 1959

2. Brode, H. L., Point Source Explosion in Air, the RAND Corporation, RM-1824, December 3, 1956

3. From theoretical work by H. L. Brode, The RAND Corporation, September 2, 1959

4. From report by J. F. Moulton, Jr., March 1960

5. Shapiro, A. H., The Dynamics and Thermodynamics of Compressible Fluid Flow, Vol. I, Ronald Press, New York, 1953

6. Sykes, D. M., Supersonic and Low Speed Flows Past Circular Cylinders of Finite Length Supported at One End, Journal of Fluid Mechanics, Vol. 12, (1962)

7. Marks, L. S., editor, Mechanical Engineer's Handbook, Fifth Edition, McGraw-Hill Book Company, New York

8. Shaw, M. C., Metal Cutting Principles, Third Edition, M.I.T., Cambridge, Massachusetts, 1954

9. Private communication, E. N. Perry, Missiles and Space Division, Lockheed Aircraft Corporation

10. May, A., and W. R. Witt, Jr., Free Flight Determination of the Drag Coefficient of Spheres, J. Aero. Sci., 635 (1953)

11. Riedel, E. G., Operational Report -- SRI-MAD Gage Test Program, prepared by AFMDC, Holloman Air Force Base, New Mexico, August 28, 1963

ACKNOWLEDGMENTS

The Institute is indebted to Lt. Colonel C. C. Clifford and Mr. J. R. Kelso of Headquarters, Defense Atomic Support Agency for their cooperation and advice in conducting this project.

We also wish to acknowledge and express our thanks for the enthusiastic support provided by the Track Test Division and their associated agencies at the Air Force Missile Development Center, Holloman Air Force Base, New Mexico.

Mr. Fred M. Sauer of the Institute staff assisted in the planning stages and the research was conducted under the supervision of Dr. E. G. Chilton. Other Institute personnel closely involved include Mr. E. E. Spitzer, mechanical design; C. T. Vincent, J. A. Kochly, R. E. Fitzgerald, and W. L. Nevarez, instrumentation and testing; and W. Lai, development of the electrical analog. Mrs. Patricia Ogle assisted in the reduction and presentation of the data and Miss Paula Truesdell helped in the preparation of the final report.

NOMENCLATURE

a	acceleration or dust particle radius
A	projected or cross-sectional area
c	distance from neutral axis to extreme fiber or sonic velocity
C_D	drag coefficient
e	capture efficiency, defined as the ratio of the actual capture rate to the capture rate if particles were not deflected from straight line trajectories
E	modulus of elasticity
f_n	natural frequency
F	force
F_D	drag force
g	unit of acceleration = 32.2 ft/sec^2
g_c	proportionality constant = 32.2 $\frac{ft\text{-}lbm}{lbf\ sec^2}$
h	target cylinder wall thickness
I	moment of inertia
K	spring rate
ℓ	length or shock detachment distance
lbf	pound force
lbm	pound mass
m	mass
M	moment or Mach number
N	dust registry coefficient
N_R	Reynolds number
I	moment of inertia
P	pressure
P_o	total pressur
P_s	static pressu
q	dynamic press
Q	volume flow r
q_{tot}	total air dyn
r	radius
s	arc length
t	thickness or
T	absolute temp
v	dust particle
V	air velocity
w	mass flow rat
W_{max}	loading parame
x	distance behi
Z	section modulu
α	angle of attac
δ	deflection
Δ	difference
ϵ	strain
λ_s	Stoke's law st
μ	viscosity
ρ	density
σ	stress

P_o	total pressure
P_s	static pressure
q	dynamic pressure
Q	volume flow rate
q_{tot}	total air dynamic pressure plus dust momentum flux
r	radius
s	arc length
t	thickness or time
T	absolute temperature (RANKINE)
v	dust particle velocity
V	air velocity
w	mass flow rate or beam loading per unit length
W_{max}	loading parameter
x	distance behind the shock wave
Z	section modulus
α	angle of attack
δ	deflection
Δ	difference
ϵ	strain
λ_s	Stoke's law stopping distance
μ	viscosity
ρ	density
σ	stress
τ	$\frac{V_1 t}{\lambda_s}$
Φ	momentum flux

Subscripts

1	free stream
2	behind the shock
a	air
d	dust
f	front port
r	rear port
g	ground
m	mixture
N	normal
s	static
S	shear

STANFORD
RESEARCH
INSTITUTE

MENLO PARK
CALIFORNIA

Regional Offices and Laboratories

Southern California Laboratories
820 Mission Street
South Pasadena, California

Washington Office
808-17th Street, N.W.
Washington 6, D.C.

New York Office
270 Park Avenue, Room 1770
New York 17, New York

Detroit Office
1025 East Maple Road
Birmingham, Michigan

European Office
Pelikanstrasse 37
Zurich 1, Switzerland

Japan Office
c o Nomura Securities Co., Ltd.
1–1 Nihonbashidori, Chuo-ku
Tokyo, Japan

Representatives

Toronto, Ontario, Canada
Cyril A. Ing
Room 710, 67 Yonge St.
Toronto 1, Ontario, Canada

Milan, Italy
Lorenzo Franceschini
Via Macedonio Melloni, 49
Milano, Italy